Survival probabilities of atmospheric particles: comparison based on theory, cluster population simulations, and observations in Beijing

Santeri Tuovinen[1], Runlong Cai[1], Veli-Matti Kerminen[1], Markku Kulmala[1], Jingkun Jiang[3], Chao Yan[1,4] and Jenni Kontkanen[1,2]

5 [1]Institute for Atmospheric and Earth System Research/Physics, Faculty of Science, University of Helsinki, Helsinki, Finland
[2]CSC – IT Center for Science, Espoo, Finland
[3]State Key Joint Laboratory of Environment Simulation and Pollution Control, School of Environment, Tsinghua University, Beijing, China
[4]Joint International research Laboratory of Atmospheric and Earth System Research (JirLATEST), School of Atmospheric
10 Sciences, Nanjing University, Nanjing, China

Correspondence to: Markku Kulmala (markku.kulmala@helsinki.fi)

Abstract

Atmospheric new particle formation (NPF) events are regularly observed in urban Beijing, despite high concentrations of
15 background particles which, based on theory, should inhibit NPF due to high values of coagulation sink (CoagS). The survival probability, which depends on both CoagS and particle growth rate (GR) is a key parameter in determining occurrence of NPF events, as it describes the fraction of newly formed particles that survive from a smaller diameter to a larger diameter. In this study, we investigate and compare survival probabilities from 1.5 to 3 nm ($J_3/J_{1.5}$), from 3 to 6 nm (J_6/J_3) and from 6 to 10 nm (J_{10}/J_6) based on analytical formulae, cluster population simulations, and atmospheric
20 observations from Beijing. We find that survival probabilities based on the cluster population simulations and one of the analytical formulae are in a good agreement. However, at low ratios between the background condensation sink (CS) and GR, and at high concentrations of sub-3 nm clusters, cluster-cluster collisions efficiently lower survival probabilities in the cluster population simulations. Due to the large concentrations of clusters and small particles required to considerably affect the survival probabilities, we consider it unlikely that cluster-cluster collisions significantly affect atmospheric survival
25 probabilities. The values of J_{10}/J_6 observed in Beijing show high variability, most likely due to influences of primary particle emissions, but are on average in a relatively good agreement with the values based on the simulations and the analytical formula. The observed values of J_6/J_3 are mostly lower than those predicted based on the simulations and the analytical formula, which could be explained by uncertainties in CS and GR. The observed values of $J_3/J_{1.5}$ at high CS/GR are much higher than predicted based on the simulations and the analytical formula. We argue that uncertainties in GR or CS are
30 unlikely to solely explain the observed values of $J_3/J_{1.5}$ under high CS conditions. Thus, further work is needed to better understand the factors influencing survival probabilities of sub-3 nm atmospheric particles in polluted environments.

1 Introduction

Atmospheric new particle formation (NPF), consisting of the formation of stable clusters and their following growth to larger sizes by the condensation of precursor vapors, has been frequently observed in many different environments (Kerminen et al., 2018). Aerosol particles affect both climate and human health (Pöschl, 2005; Rosenfeld et al., 2014; Shiraiwa et al., 2017; Bellouin et al., 2020) and NPF events significantly contribute to atmospheric concentrations of aerosol particles (Spracklen et al., 2010). Thus, NPF events can influence the effects of aerosol particles on climate and health. For example, they can increase the cloud condensation nuclei concentrations, thereby influencing climate and other properties of clouds (Spracklen et al., 2008; Yue et al., 2011). In addition, NPF events can contribute to haze episodes and lead to a degrading air quality (Guo et al., 2014; Kulmala et al., 2021, 2022).

The survival probability of molecular clusters and small aerosol particles is one of the key parameters that determine whether an NPF event occurs or not. It also determines the fraction of newly formed clusters, which are eventually able to contribute to the pre-existing particle population, and thereby potentially affect haze and aerosol-cloud interactions. In practice, the survival probability describes the fraction of particles or clusters formed at diameter d_1 that grow to a larger diameter d_2. It can be determined as the ratio of the formation rates of particles of diameters d_1 and d_2 (Pierce and Adams, 2007; Kulmala et al., 2017). The survival probability is governed by the growth rate (GR) and loss rate of small particles and clusters (Kerminen and Kulmala, 2002; Kulmala et al., 2017). GR depends on the concentrations of condensable precursor vapors (Kulmala et al., 2005; Sihto et al., 2006; Wang et al., 2015; Stolzenburg et al., 2020) and population dynamics such as cluster-cluster collisions (Kontkanen et al., 2022). The losses of atmospheric new particles can be characterized by the coagulation sink, denoted by CoagS, which describes the loss rate of small particles to larger particles by coagulation (Dal Maso et al., 2002; Kulmala et al., 2001). The value of CoagS depends on the diameter of the particle and is higher for smaller particles (Kulmala et al., 2001; Dal Maso et al., 2002). Condensation sink, denoted by CS, describes the loss rate of condensable vapor, often sulfuric acid, on particles, and it is often used as a proxy for the CoagS (Dal Maso et al., 2002; Kerminen and Kulmala, 2002). If the ratio of CoagS, or CS, to GR is low, the survival probability is high and high fractions of small particles are able into survive to larger sizes (Kulmala et al., 2017). This can result in an NPF event being observed if the initial concentrations of clusters are sufficiently high.

In this study, we focus on the survival of new particles in the polluted atmosphere in Beijing, China, where NPF events have been observed to occur frequently despite the high CoagS (Chu et al., 2019; Deng et al., 2020; Cai et al., 2021b). The median CS during NPF days in Beijing was found to be ~0.02 s^{-1} (Deng et al., 2020; Wu et al., 2008; Zhou et al., 2020). Previous studies have shown that the survival probabilities in Beijing and other megacities are significantly higher than theoretically predicted under high CoagS and CS conditions (Kulmala et al., 2017; Yao et al., 2018). For example, in Beijing NPF events have been observed to occur even when the ratio of CS to GR is so high (e.g., > 50 nm^{-1}) that theoretically no formation of 3

65 nm particles should be possible (Kulmala et al., 2017). This indicates a gap in the current understanding of NPF and this is why the survival probabilities of small particles in polluted environments are of high interest.

Here, we will investigate survival probabilities in the diameter ranges 1.5 – 3 nm, 3 – 6 nm and 6 – 10 nm based on observations from Beijing, cluster populations simulations using Atmospheric Cluster Dynamics Code (ACDC) (McGrath et

70 al., 2012; Olenius and Riipinen, 2017), and analytical formulae. Three different size ranges of the survival probability will be investigated, as motivated by the size-dependency of the survival probability (Kerminen and Kulmala, 2002) in order to find out whether there is an agreement between the observations, simulations, and analytical formulae, and how this depends on the size range. The observations are based on particle number size distribution measurements from one year (2018), from which CS, GR and the formation rates of 1.5 nm, 3 nm, 6 nm and 10 nm particles will be derived. The formation rates will

75 then be used to determine survival probabilities. Cluster populations simulations allow considering the effects of particle population dynamics on survival probabilities (Kontkanen et al., 2022). Two different sets of simulations will be conducted: first assuming that there are no collisions between newly formed particles (i.e. particles grow only by collisions of vapor molecules) and then allowing collisions between new particles to occur. Theoretical predictions for survival probabilities will be determined according to analytical formulae by Kerminen and Kulmala (2002), Lehtinen et al. (2007), and Korhonen

80 et al. (2014). These equations relate the formation rate at a larger diameter to the formation rate at a smaller diameter, and since survival probability can be expressed as a ratio of formation rates, they can be used to determine survival probabilities from a smaller diameter to a larger diameter. The difference between the equations by Lehtinen et al. (2007) and Korhonen et al. (2014) is that the former assumes a constant GR while the latter assumes a linear or a power-law dependency of the GR on the particle diameter. Kerminen and Kulmala (2002) equation also assumes a constant GR, however it differs from the

85 equation by Lehtinen et al. (2007) by relying on CS instead of CoagS and by handling the size-dependency of the sink term differently.

The main objectives of this study are 1) to investigate if, and how, the survival probabilities of sub-10 nm particles differ

90 between observations, cluster population simulations and analytical formulae, 2) to evaluate the effect of uncertainties in the observed parameters on our results, and to 3) discuss other possible explanations, such as ineffective CoagS or enhanced GR. In practice, we will first compare theoretical survival probabilities, the survival probabilities from cluster population simulations, both with and without cluster-cluster collisions, and the observed survival probabilities. Then we will investigate how large of an uncertainty in GR or CS is needed to explain the observed survival probabilities and consider

95 some reasons for inaccuracy of CoagS and GR, including the measurement uncertainty and some assumptions made in determining CoagS or GR. Finally, other explanations for our results will be briefly discussed. Based on our results we can get a better understanding of NPF in polluted megacities and gain more insight into the reasons behind disagreements between the predicted and observed survival probabilities.

2 Methods

2.1 Theoretical survival probability

The survival probability of atmospheric particles or clusters describes the probability, or fraction, of particles of a smaller diameter d_1 growing to a larger diameter d_2 (Pierce and Adams, 2007). In other words, it is the probability that a growing particle, initially of diameter d_1, is not lost due to coagulation scavenging and other loss mechanisms, such as dry deposition, before it reaches the diameter d_2. Coagulation scavenging, described by the coagulation sink (CoagS) is usually the most important sink for sub-10 nm particles, and in this study, it is the only loss mechanism of particles we consider.

The survival probability can be expressed as the ratio of the formation rates J_1 and J_2 (Kulmala et al., 2017). In this study three different survival probabilities were considered: that from 1.5 to 3 nm ($J_3/J_{1.5}$), that from 3 to 6 nm (J_6/J_3), and that from 6 to 10 nm (J_{10}/J_6). Based on Kerminen and Kulmala (2002), the survival probability against coagulation scavenging from d_1 to d_2 is

$$\frac{J_2}{J_1} = \exp\left[\eta \frac{CS'}{GR}\left(\frac{1}{d_2} - \frac{1}{d_1}\right)\right] \quad , \tag{1}$$

where GR is the growth rate between d_1 and d_2 and CS' = CS/($4\pi D$). CS is the condensation sink of sulfuric acid and D is the diffusion coefficient of sulfuric acid. CS is used as a proxy for the coagulation sink (CoagS). Parameter η is a semi-empirically derived quantity taking into account the influence of the background particle size distribution on the size-dependency of the CoagS. It is approximately equal to 0.23 $nm^2\ m^2\ h^{-1}$.

The survival probability can also be determined based on the formulations by Lehtinen et al. (2007) and Korhonen et al. (2014), which directly use the CoagS instead of the CS to describe the particle scavenging losses. Based on these two studies, J_2/J_1 can be written as

$$\frac{J_2}{J_1} = \exp\left(-\gamma d_1 \frac{CoagS_1}{GR}\right) \quad , \tag{2}$$

where $CoagS_1$ is the coagulation sink at the smaller diameter d_1. If J_2/J_1 is determined based on Lehtinen et al. (2007), the growth rate (GR) is assumed to be constant, GR = GR_{1-2}, and GR_{1-2} is the growth rate from the smaller diameter d_1 to the larger diameter d_2. In this case

$$\gamma = \frac{1}{m+1}\left[\left(\frac{d_2}{d_1}\right)^{m+1} - 1\right]. \tag{3}$$

Here, the parameter m depends on the background particle distribution, and it is defined as

$$m = \frac{\log(CoagS_2/CoagS_1)}{\log(d_2/d_1)} \quad . \tag{4}$$

CoagS$_2$ is the coagulation sink of the larger particle with diameter d_2. In this work, if not otherwise stated, we assume that m = −1.6 when making predictions for the survival probabilities based on the analytical formulae. The effects of this assumption will be considered in Sect. 3.2, where the sensitivity of the survival probability on m are briefly investigated.

If the survival probability is determined based on Korhonen et al. (2014), GR is either assumed to have a linear or power-law size dependency on the particle diameter. In this study, we only considered the case with power-law size dependency, in which case GR in Eq. 2 is the growth rate at the smaller size d_1, GR = GR$_1$, and

$$\gamma = \frac{1}{m-n+1}\left[\left(\frac{d_2}{d_1}\right)^{m-n+1} - 1\right] \quad . \tag{5}$$

The parameter n, related to the size dependency of GR, is analogous to the parameter m, and it is defined as

$$n = \frac{\log\left(\mathrm{GR}_2/\mathrm{GR}_1\right)}{\log\left(d_2/d_1\right)} \quad , \tag{6}$$

where GR$_2$ is the growth rate at diameter d_2.

From here on, we will refer to the predicted survival probabilities based on Kerminen and Kulmala (2002), Lehtinen et al. (2007) and Korhonen et al. (2014) with KK-2002, L-2007 and K-2014.

2.2 Formation rate of atmospheric clusters and particles

The particle formation rate (J_i) is one of the parameters used to characterize NPF. It describes the flux of growing particles past some diameter d_i. Using the formulation derived based on the aerosol general dynamic equation, J_i can be determined from the particle number size distribution using (Kulmala et al., 2012)

$$J_i = \frac{\mathrm{d}\,N_{[d_i,d_u)}}{\mathrm{dt}} + \mathrm{CoagS}\cdot N_{[d_i,d_u)} + \frac{\mathrm{GR}_{[d_i,d_u)}}{d_u-d_i}N_{[d_i,d_u)} \quad . \tag{7}$$

Here, $N_{[d_i,d_u)}$ is the particle number concentration between diameters d_i and d_u, excluding the upper limit d_u. $\mathrm{GR}_{[d_i,d_u)}$ is the growth rate and CoagS is the coagulation sink of the particles in the size range. To account for the coagulation effects and their influence on J_i more accurately J_i can be calculated based on an improved formulation of Eq. 7 proposed by Cai and Jiang (2017)

$$J_i = \frac{\mathrm{d}\,N_{[d_i,d_u)}}{\mathrm{d}\,t} + \sum_{d_g=d_i}^{d_{u-1}}\sum_{d_j=d_{min}}^{+\infty} K_{(j,g)}N_{[d_j,d_{j+1})}N_{[d_g,d_{g+1})} - \frac{1}{2}\sum_{d_g=d_{min}}^{d_{u-1}}\sum_{d_j=max(d_{min}^3,d_i^3-d_{min}^3)}^{d_{j+1}^3+d_{g+1}^3\leqslant d_u^3} N_{[d_j,d_{j+1})}N_{[d_g,d_{g+1})} + n_u\cdot\mathrm{GR}_\mathrm{u}. \tag{8}$$

Here, d_j is the lower limit of jth measured size bin, $K_{(j,g)}$ is the coagulation coefficient for collisions between particles with diameters d_j and d_g, d_{min} is the lowest measured particle diameter, n_u is the particle size distribution function and GR$_\mathrm{u}$ is the growth rate at d_u.

2.3 Growth rate and condensation and coagulation sinks

The particle growth rate (GR) describes the rate of change of particle diameter with time. In this study, the value of GR was determined using the appearance time method (Lehtipalo et al., 2014; Olenius et al., 2014). This method is based on finding a corresponding time of appearance ($t_{app,i}$) for each particle size bin i, usually defined as the time that the number

150   concentration in that size bin reaches 50% of its maximum value during a NPF event. The GR is then estimated using the slope of the diameters versus the corresponding t_{app}

$$\text{GR} = \frac{\Delta d_i}{\Delta t_{app,i}} \quad . \tag{9}$$

GR derived from the appearance times can be affected by processes other than the particle growth such as coagulation scavenging, which can lead to an overestimation of GR (Stolzenburg et al., 2005; Cai et al., 2021a). Thus, in this work GR was corrected for the influence of background CoagS according to the procedure presented by Cai et al. (2021a).

155

CS, which describes the loss rate of condensing vapor to background particles, can be determined from the particle number size distribution (Dal Maso et al., 2002)

$$\text{CS} = 2\pi D \sum_j \beta_j N_j d_j \quad , \tag{10}$$

where β_j is the transition regime correction factor (Fuchs and Sutugin, 1971). CoagS_i, which describes the loss rate of small particles of diameter d_i to larger background particles, is obtained from the following equation:

$$\text{CoagS}_i = \sum_j K_{i,j} N_j \quad , \tag{11}$$

160   where $K_{i,j}$ is the coagulation coefficient between collisions of the particles i and j. Due to the similar dependency on the particle number size distribution, CoagS can be determined from the CS using the parameter m, which was introduced in Sect 2.1. Thus,

$$\text{CoagS}_i = \text{CS} \times \left(\frac{d_i}{d_{mon}}\right)^m \quad , \tag{12}$$

where d_{mon} is the diameter of the condensing monomer. Because of this relation between the CS and the CoagS, and the size dependency of the CoagS, we have chosen to use CS/GR (nm^{-1}), where the CS is for sulfuric acid, to represent the ratio

165   between coagulation scavenging and particle growth. The survival probabilities in this study will thus be presented with respect to CS/GR.

2.4 Cluster population simulations

We investigated the agreement between survival probabilities from analytical formulae and cluster population simulations using Atmospheric Cluster Dynamics Code (ACDC). These simulations were used as an intermediate step between the

170   theory and the atmospheric observations. The ACDC program models the first steps of the atmospheric cluster and particle

formation by solving the aerosol general dynamic equation (McGrath et al., 2012; Olenius and Riipinen, 2017):

$$\frac{dN_i}{dt} = \frac{1}{2}\sum_{j<i} K_{j,(i-j)}N_j N_{(i-j)} + \sum_j E_{(i+j)\to i}N_{i+j} - \sum_j K_{i,j}N_i N_j - \frac{1}{2}\sum_{j<i} E_{i\to j}N_i + Q_i - \text{CoagS}_i N_i - S_i,$$
(13)

where $K_{i,j}$ is the coagulation coefficient between collisions of clusters or i and j, $E_{i\to j}$ is the evaporation coefficient from the

cluster i to two smaller clusters, the other of which is the cluster j. Q_i describes external sources of clusters i while S_i

describes their external losses, such as wall losses, other than CoagS_i, which describes the coagulation losses of clusters to a

175   background particle population. In our simulations Q_i and S_i were set to zero. The coagulation coefficients were determined

assuming hard sphere collisions with an accommodation (sticking) factor of unity. Note that in this study particles and

clusters are referred as clusters, regardless of their size, when concerning the cluster population simulations.

We assumed monomer of the model substance to have properties corresponding to a cluster consisting of one sulfuric acid

180   and one dimethylamine molecule, similar to the approach by Kontkanen et al., (2018). This corresponds to a situation where

every sulfuric acid molecule is bound to a dimethylamine molecule. The formation of clusters was assumed to be irreversible

and thus, in Eq. 13 $E = 0$. Sulfuric acid and dimethylamine cluster formation has been observed to be the main pathway of

the initial formation of atmospheric clusters in Beijing (Cai et al., 2021b). Evaporation in the cluster formation from sulfuric

acid and dimethylamine has been observed to be negligible (Jen et al., 2014; Kürten et al., 2014).

185

Two different simulation sets were considered. In the first simulation set, further on referred to as Case 1, collisions only

occurred between the monomers and the clusters, which means that in Eq. 13 $K_{i,j} \neq 0$, only when the cluster j is the

monomer ($j = 1$). In the second simulation set, referred as Case 2, collisions between the clusters were also allowed to occur.

Thus, while in Case 1 the cluster growth was only due to condensation, in Case 2 smaller clusters also contributed to the

190   growth and, at the same time, larger clusters contributed to the losses of the smaller clusters.

The monomer concentration (C_{mon}) was kept constant during all the simulations at $C_{mon} = 1\cdot10^7$ cm^{-3}, the value of which was

chosen based on previous studies of sulfuric acid concentrations in Beijing (Yue et al., 2010; Lu et al., 2019; Li et al., 2020).

The largest modeled clusters consisted of 4000 monomers and were above 10 nm in diameter. The background CS of the

195   monomer, which was given as an input to the program, was varied between $5\cdot10^{-4}$ s^{-1} and 0.02 s^{-1} within the simulation sets.

The model calculated the corresponding background CoagS of clusters based on Eq. 12. The properties of the monomer and

other constant properties are presented in Table 1. We note that while the typical CS in Beijing is much higher than the

lowest CS values used in this study, we have selected them so that the resulting CS/GR values are in a comparable range

with the observed values.

200

ACDC was run until steady-state, i.e., until the concentrations of clusters with diameters up to 10 nm did not considerably change with time anymore ($\mathrm{d}N_i/\mathrm{d}t \approx 0$). The cluster formation rates at the diameters 1.5 nm, 3 nm, 6 nm and 10 nm, which we needed to determine the survival probabilities, were returned by the program as the cluster flux past these sizes. In addition, formation rates were also determined based on Eq. 7. Steady-state formation rates from Eq. 7 were determined using the concentrations in different size bins, which the program returned as an output file. Since the particle size distributions are at the steady-state, the change of the cluster concentration with time is zero in Eq. 7. The upper d_u limit for $J_{1.5}$, J_3 and J_6 is 10 nm, and for J_{10} it was 10.7 nm, corresponding to the largest clusters with non-zero number concentrations in the system.

The GR was determined based on the appearance time method (see Sect. 2.3). Both polynomial regression and linear regression with three size ranges (1.5-3 nm, 3-6 nm, 6-10 nm) were used to determine GR from the appearance times. Unless otherwise stated, the values of GR presented in this study are based on polynomial regression due to the strong size-dependency of GR, and if a constant GR is used, such as for the ratio CS/GR, it is based on arithmetic mean GR.

Table 1: Temperature (T), ambient pressure (P), vapor monomer concentration (C_{mon}), vapor monomer mass (m_{mon}) and vapor monomer density (ρ_{mon}) used in Atmospheric Cluster Dynamics Code simulations in this study.

Property	Value
P	1 atm
T	278 K
C_{mon}	10^7 cm^{-3}
m_{mon}	143.1590 g/mol
ρ_{mon}	1500 kg m^{-3}

2.5 Measured survival probability in Beijing

In this work we used measured particle number size distributions and measurement-based values of CS, GR and formation rates from Beijing to determine the survival probabilities $J_3/J_{1.5}$, J_6/J_3 and J_{10}/J_6 and the corresponding ratios between CS and GR. All the data were based on measurements at the station of Beijing University of Chemical Technology (39°56'31"N, 116°17'50"E, Beijing) during 2018. The particle number size distribution between 1 nm and 1 μm were measured with a Diethylene Glycol Scanning Mobility Particle Sizer and a custom-made Particle Size Distribution system (Jiang et al., 2011; Liu et al., 2016; Cai et al., 2017a). The formation rates for 1.5 nm ($J_{1.5}$), 3 nm (J_3), 6 nm (J_6) and 10 nm (J_{10}) particles were

determined using Eq. 8. The upper limit for the determination of formation rate, d_u, were 3 nm for $J_{1.5}$ and 25 nm for the other J. More details on the measurement site and measurements can be found at Zhou et al. (2020).

225 Days were classified as NPF event days if a new mode below 25 nm appeared and its growth to larger sizes was observed within the following hours (Dal Maso et al., 2005). Only the NPF event days with a clear appearance of sub-3 nm particles and growth up to over 10 nm sizes were included in the analysis. We determined the formation rates for survival probability calculation with a time-delay in order to account for the non-steady state aerosol size distributions during NPF. The time delay between the formation of particle of diameter d_1 and particle of diameter d_2 was determined based on the GR between

230 these two sizes,

$$\Delta t_{1-2} = (d_2 - d_1)/\mathrm{GR}_{1-2} \quad . \tag{13}$$

This time delay was then used to choose the formation rate at d_2 (J_2) corresponding to formation rate at the diameter d_1 (J_1). Thus, survival probability from d_1 to d_2 is

$$\frac{J_2}{J_1} = \frac{J_2(t_1 + \Delta t_{1-2})}{J_1(t_1)} \quad . \tag{14}$$

The value of CS for the ratio CS/GR corresponding to the survival probability was calculated as the median value between t_1 and t_2. All the times were chosen so that the earliest and the last $J_{1.5}$ value from the day corresponded to approximate start

235 and end of formation of 1.5 nm particles, which were based on a visual analysis of the event day particle number size distributions. We used only one daily GR value for a certain size range and assumed that throughout the day GR from a smaller size d_1 to a larger size d_2 remains the same. In addition to inaccuracies in CS/GR, this assumption also affects the values of the survival probabilities themselves as we have used the GR to select the formation rates. The atmospheric particle GR can be expected to vary, for example due to changes in the concentrations of different condensing vapors.

240

The values of GR were determined based on the appearance time method (see Sect 2.3) and they were determined based on linear regression for limits $1.5 - 3$ nm ($\mathrm{GR}_{1.5-3}$), $3 - 7$ nm (GR_{3-7}), and 7 nm $- 25$ nm (GR_{7-25}). For calculating the survival probabilities $J_3/J_{1.5}$ and J_6/J_3 $\mathrm{GR}_{1.5-3}$ and GR_{3-7} were used, respectively, whereas for calculating J_{10}/J_6 the weighted mean value of GR_{3-7} and GR_{7-25} was used. These same values of GR were also used to determine CS/GR corresponding to the survival

245 probabilities.

3 Results and discussion

3.1 Formation rates and growth rates in cluster population simulations

Figure 1 shows GRs based on multi-degree polynomial regression from the cluster population simulations for both Case 1 and Case 2 for different input background CS. In Case 1 collisions between clusters did not occur while in Case 2 they did.

250 In Case 1, GR has very similar values at all CS values since growth only occurs through condensation and C_{mon} is constant. GR depends on d_i so that smaller d_i has a larger GR. This size dependency is stronger at smaller diameters while for larger d_i GR is almost constant. Such observed behavior of GR in the simulations for Case 1 results from the coalescence with the monomer increasing the size of a smaller cluster relatively more than that of a larger cluster (Nieminen et al., 2010).

255 Figure 1 also shows GR for Case 2. When including cluster-cluster collisions, GR as a function of d_i shows very different behavior depending on the background CS. When CS is small, GR is much higher for all the cluster sizes compared to Case 1. With increasing CS, GR becomes smaller with the change being larger for larger d_i. If CS=0.02 s^{-1}, GR is significantly larger for Case 2 compared to Case 1 at small d_i, the difference being over 1 nm/h at d_i = 1.5 nm. With the same background CS, the difference in GR for the two cases is approximately 0.2 nm/h at d_i > 3 nm. In Case 2 the GR depends strongly on
260 background CS since at smaller background CS the concentrations of clusters are higher and the cluster-cluster collisions contribute more to the growth. On the contrary, when the background CS is larger, the cluster concentrations remain small and the effect of cluster-cluster collisions on the cluster growth remains minor. The cluster GR can be significantly enhanced by cluster-cluster collisions if the cluster concentrations are sufficiently high in comparison to CS. Lehtipalo et al. (2016) have previously shown that if the concentrations of stabilizing vapors such as dimethylamine are high, resulting in low or
265 negligible evaporation rates, cluster-cluster collisions can have a major contribution to the growth of clusters and particles, especially if CS is low. The same has also been observed in studies utilizing cluster population simulations (Kontkanen et al., 2022).

It should be noted that while we do not explicitly account for the effect of cluster-cluster collisions on the coagulation losses
270 of the clusters in this study, the loss rates of the clusters can also be considerably affected by the cluster-cluster collisions in addition to the GRs if the background CS is small and the cluster concentrations are high.

ACDC determines the output formation rates directly based on the cluster growth fluxes over the threshold diameters, whereas the formation rates from the atmospheric observations are determined based on the measured particle number size
275 distribution (see Sect 2.2). To investigate whether this difference in method to determine formation rate could result in disagreements between the cluster population simulations and the observations, we compared the cluster population model steady-state formation rates from the fluxes to the formation rates calculated based on Eq. 7 for the case with no cluster-cluster collisions.

280 Figure 2 shows that for all the sizes, the two formation rates are approximately within a factor of two. J_3, J_6 and J_{10} are very close to the same value despite the method it is determined with. However, the majority of the values of $J_{1.5}$ are smaller if the formation rates have been determined based on Eq. 7 compared to if they are based on the fluxes. Thus, whether we determine formation rate based on fluxes or Eq. 7 does not cause a significant difference in the values of J_{10}/J_6 or J_6/J_3.

Determining $J_3/J_{1.5}$ based on the formation rates from Eq. 7 results in a larger value compared to if the formation rates are

285 directly based on the cluster growth fluxes. However, the differences are relatively minor, and thus we assume that they do not affect our results and conclusions considerably.

3.2 Sensitivity of survival probability on CS/GR and m-parameter

We investigated the sensitivity of L-2007 survival probability to the ratio CS/GR and the parameter *m*. Figure 3 illustrates the sensitivity of the survival probabilities to CS/GR and shows how uncertainties in CS, or GR, can lead to disagreements

290 between the observed survival probability and theoretical survival probability. For example, if CS/GR is 40, $J_3/J_{1.5}$ can be underestimated by almost three orders of magnitude if the true CS/GR is 50% of the assumed value. Similarly, if the true CS/GR is 50% larger than the assumed CS/GR of 40, we can overestimate $J_3/J_{1.5}$ by two orders of magnitude. The survival probability is less sensitive to CS/GR when CS/GR is low, and thus the error in CS/GR results in a larger error in the survival probability at high CS/GR. If either the GR or CS determined based on measurements is inaccurate, the predicted

295 theoretical survival probability can be significantly different from the one we observe. This is especially true for highly polluted environments where CS/GR is often quite high.

Additionally, we investigated the sensitivity of L-2007 survival probability to the parameter *m* (Figure 4). J_6/J_3 and J_{10}/J_6 are more sensitive to *m* than $J_3/J_{1.5}$. The parameter *m* varies to some extent as the number size distribution of larger particles

300 changes, which can also affect the survival probability of particles or clusters. For example, when CS/GR is around 20, J_6/J_3 is approximately 0.02, 0.05 and 0.08 when $m = -1.4$, -1.5 and -1.6 respectively. However, considering the uncertainties associated with the measured formation rates, CS and GR, we may assume that the effect of our assumption that $m= -1.6$ on our results is relatively minor. We further discuss this in Sect. 3.4.

3.3 Survival probabilities in cluster population model simulations

305 Figure 5 shows the survival probabilities $J_3/J_{1.5}$, J_6/J_3 and J_{10}/J_6 based on the cluster population model simulations and analytical formulae (see Sect 2.1) as a function of CS/GR. In addition, $J_{10}/J_{1.5}$ based on the cluster population model simulations is shown. Note that CS in CS/GR is the background CS, which for the ACDC Case 1 corresponds to the total loss rate. The ratio CS/GR corresponding to the values of survival probabilities from the cluster population model simulations was determined by appearance time method based on both linear and multi-degree polynomial regression (see

310 Sect 2.3 and Sect 2.4).

We see that for Case 1 with no cluster-cluster collisions, the ratio CS/GR corresponding to a value of the survival probability $J_3/J_{1.5}$ is higher if GR is based on the linear regression of the appearance times than on multi-degree polynomial regression, which is especially apparent at higher CS. As GR is highly size-dependent at smaller diameters, determining it based on the

315 linear fit leads to a higher uncertainty in GR between 1.5 and 3 nm. This underestimation of GR increases $J_3/J_{1.5}$ at certain

CS/GR. While GR based on the linear regression of the appearance times is at most approximately 30% lower than GR based on the multi-degree polynomial regression of the appearance times, the effect on the interpretation of our results is significant: at similar CS/GR the value of $J_3/J_{1.5}$ can seem to be much higher. Similar observations can be made about ACDC Case 2 with cluster-cluster collisions at high CS. As discussed in Sect 3.2, survival probabilities are highly sensitive to uncertainties in CS and GR, and thus GR should always be determined as accurately as possible. For this reason, further discussion of the cluster population model survival probabilities is focused on the results with GR based on the multi-degree polynomial regression of the appearance times.

For Case 1 with no cluster-cluster collisions, we can see that $J_3/J_{1.5}$ from the cluster population simulations is higher than the KK-2002 $J_3/J_{1.5}$, however the difference is relatively small. J_6/J_3 and J_{10}/J_6 from the simulations are considerably lower than the KK-2002 J_6/J_3 and J_{10}/J_6. The L-2007 survival probabilities are closer to the cluster population simulation survival probabilities and the only notable, but still relatively small, differences are observed at high CS/GR for $J_3/J_{1.5}$ and J_6/J_3. The ACDC Case 1 $J_3/J_{1.5}$ is higher than the L-2007 $J_3/J_{1.5}$ by a bit more than a factor of two at its largest.

The differences in the KK-2002 and the L-2007 survival probabilities are due to the formula by Kerminen and Kulmala (2002) having a less accurate size-dependency of CoagS. This is because in the derivation of the formula by Kerminen and Kulmala (2002), a power-law dependency of CoagS with an exponent of −2 was assumed. The assumption is then corrected by a semi-empirically derived correction parameter, while the Lehtinen et al. (2007) formulation directly accounts for the size-dependency of CoagS.

Both the KK-2002 and the L-2007 survival probabilities are determined using a constant GR, which in this case is the arithmetic mean GR in the relevant size-range. Since GR for Case 1 in the cluster population simulations is highly size-dependent (see Figure 1), the small differences between the L-2007 and the ACDC Case 1 survival probabilities are likely explained by this assumption of a constant GR. This is supported by the K-2014 survival probabilities, which were determined assuming a power-law size dependency of GR, being approximately the survival probabilities from the cluster population simulations for the three size-ranges.

Figure 5 shows $J_3/J_{1.5}$, J_6/J_3 and J_{10}/J_6 for ACDC Case 2. In Case 2 collisions between clusters occurred in addition to the collisions between the monomers and the clusters. We see that for larger CS/GR the behavior of the survival probabilities is similar to Case 1. However, for CS/GR roughly below 20, $J_3/J_{1.5}$, J_6/J_3 and J_{10}/J_6 are considerably smaller than the survival probabilities based on the analytical formulae and from Case 1. The Case 2 $J_3/J_{1.5}$ is smaller than the Case 1 $J_3/J_{1.5}$ by more than an order of magnitude when CS/GR < 7. In addition, Figure 5 shows $J_{10}/J_{1.5}$ for both Case 1 and Case 2. It is clear that the survival rates from 1.5 up to 10 nm are considerably decreased by cluster-cluster collisions when background CS is low. This is because when CS is low and the concentrations of clusters are high, cluster-cluster collisions reduce the number

350 concentrations more efficiently than they increase the survivability of clusters from coagulation scavenging due to enhanced growth. Similar decrease in survival probabilities due to high numbers of collisions between clusters has been previously shown in model simulations and CLOUD chamber experiments by Xiao et al. (2021).

Based on our results we cannot directly say whether, and to what extent, particle and cluster survival probabilities in
355 atmospheric environments are affected by cluster-cluster collisions. However, we have shown that if the concentrations of sub-10 nm particles and clusters are high, the survival probabilities can be considerably influenced by the increased loss rates. In addition, the dependency of survival probability on the background CS can be weakened due to high rates of collisions between sub-10 nm particles and clusters.

3.4 Survival probabilities in Beijing

360 ### 3.4.1 Survival probabilities during a median new particle formation event

We first show a median NPF event day in Beijing based on the investigated days in Figure 6. The median formation rates and survival probabilities for the three investigated size ranges are shown alongside the L-2007 survival probabilities (see Sect 2.1). The values of the median survival probabilities and ratio CS/GR were determined based on Eq. 14 and Eq. 15. During the median event, GR between 1.5 and 3 nm is 2.5 nm/h, between 3 and 6 nm it is 4.9 nm/h, and between 6 and 10
365 nm it is 3.4 nm/h. Between 07:00 and 14:00 (local time) the ratio CS/GR corresponding to the survival probability $J_3/J_{1.5}$ varies approximately between 8 and 11, while the CS/GR corresponding to J_6/J_3 and J_{10}/J_6 vary approximately between 4 and 6, and 6 and 8. The variability in CS/GR during the median day is quite minor, however it should be noted that the variability during separate days can be considerably larger.

370 Figure 6 illustrates how the formation rates and the survival probabilities vary during a NPF event. At first the formation rates increase during the event, reaching a peak after which they start to decrease. $J_{1.5}$ reaches the peak value first, followed by J_3, J_6 and J_{10} demonstrating the time delay between the formation of different diameters. The value of CS during the median NPF event varies little and because of the following low variability of the CS/GR, the predicted survival probabilities are relatively constant during the event. The median $J_3/J_{1.5}$ is mostly higher than the L-2007 $J_3/J_{1.5}$ except in the
375 afternoon when clusters do not appear to grow to larger sizes effectively. However, the difference is relatively small, less than by a factor of three at its highest. The median J_6/J_3 is always lower than the L-2007 J_6/J_3 and most of the time the difference is larger than for $J_3/J_{1.5}$. At its peak value, when the difference is the smallest, the median J_6/J_3 is ~70% of the predicted J_6/J_3. When the median event first is observable, the median J_{10}/J_6 is higher than the L-2007 J_{10}/J_6. However, this is likely due to influence of other sources, such as traffic emissions, on formation rates rather than due to NPF. For a large
380 fraction of the time the observed median and the L-2007 J_{10}/J_6 agree relatively well.

3.4.2 Survival probabilities and particle growth and losses

Figures 7, 8, and 9 show the observed survival probabilities $J_3/J_{1.5}$, J_6/J_3 and J_{10}/J_6 in Beijing, China, as a function of CS/GR. The survival probabilities from the cluster population simulations for both Case 1 and 2, corresponding to the cases with no collisions between the clusters and including them, are also shown for comparison. Finally, the L-2007 survival probabilities are shown. Figures 7, 8 and 9 also show J, CS and GR corresponding to the observed survival probabilities. Note that while the CS for ACDC Case 2 represents the background CoagS, and neglects the losses due to coagulation between the clusters, we assume that this does not affect the comparability to the observed survival probabilities since CS in Beijing is mostly governed by accumulation mode particles (Cai et al., 2017b).

A majority of the observed $J_3/J_{1.5}$ are larger than predicted by the L-2007 and the ACDC Case 1 and Case 2 (Figure 7). When the ratio CS/GR $\approx$ 10, the median of the observed $J_3/J_{1.5} \approx 0.2$ while the ACDC Case 1 and the L-2007 $J_3/J_{1.5} \approx 0.1$ and the ACDC Case 2 $J_3/J_{1.5} \approx 0.03$. When CS/GR $\approx$ 20, the corresponding median observed $J_3/J_{1.5} \approx 0.2$. At a similar CS/GR, ACDC Case 1 and L-2007 predict that $J_3/J_{1.5} \approx 0.01$, and the ACDC Case 2 $J_3/J_{1.5} \approx 0.005$. At CS/GR $\geq$ 20, the differences in $J_3/J_{1.5}$ between the observations and theory are considerably larger than at lower CS/GR, and a much higher fraction of the particles appears to grow from 1.5 nm to 3 nm than L-2007 or the cluster population simulations predict.

The ACDC Case 1 and the L-2007 $J_3/J_{1.5}$ have a strong exponential dependency on CS/GR, which is not apparent in the observed $J_3/J_{1.5}$. While $J_3/J_{1.5}$ appears to be on average lower when CS/GR is higher, the difference is much less than expected. The same is true for ACDC Case 2 $J_3/J_{1.5}$. It might be possible that at sufficiently low background CS, the effect of collisions with other small particles considerably decreases the atmospheric $J_3/J_{1.5}$, explaining the weak dependency of observed survival probability on CS. However, this would mean that without these additional losses due to coagulation with other small particles, the observed $J_3/J_{1.5}$ would be even higher at low CS/GR, further increasing the disagreement between the theoretical predictions and atmospheric observations. In addition, Xiao et al. (2021) showed that the van der Waals attraction force, which we have not taken into account, enhances GR and leads to a weaker dependency of survival probability on CS, which could in part explain the weak dependency of the observed $J_3/J_{1.5}$ on CS.

Unlike for $J_3/J_{1.5}$, the observed J_6/J_3 is on average lower than the L-2007 and the ACDC Case 1 J_6/J_3 (Figure 8). When CS/GR $\approx$ 5, L-2007 and the ACDC Case 1 $J_6/J_3 \approx 0.5$, while most of the observed J_6/J_3 are lower than that, and the median of the observed $J_6/J_3 \approx 0.2$. The observed J_6/J_3, like $J_3/J_{1.5}$, does not show a strong dependency on the ratio CS/GR. The ACDC Case 2 values of J_6/J_3 are smaller than most of the observed J_6/J_3, however the difference between the observed median and the ACDC Case 2 J_6/J_3 is mostly within a factor of two. In addition, the dependency on CS/GR is similar for both the observations and the ACDC Case 2 J_6/J_3 within the range of relevant values of CS/GR. Thus, the observed J_6/J_3 could be explained quite well by assuming high rates of collisions between sub-10 nm particles when CS/GR is relatively

low. The median values of the observed J_{10}/J_6 are relatively close to the values of J_{10}/J_6 based on ACDC Case 1, 2 and L-
415   2007 (Figure 9). However, the observed J_{10}/J_6 varies a lot and a notable fraction of the values are above unity. At this size
range, particle emissions from traffic can considerably affect the observed J, thereby influencing J_{10}/J_6, as indicated by by
size-resolved particle number emissions determined for the same measurement station (Kontkanen et al., 2020). We assume
that most of the variability in the observed J_{10}/J_6 can be explained by some combination of emissions of sub-10 nm particles
and measurement inaccuracies and thus our analysis and discussion focus more on J_6/J_3 and $J_3/J_{1.5}$.

420

Table 2 shows the root-mean-square logarithmic error and absolute mean error of the observed survival probabilities to the
L-2007 survival probabilities. L-2007 describing the observed J_{10}/J_6 best while the disagreement is highest for $J_3/J_{1.5}$. It is
also clear that L-2007 is closer in describing the observed $J_3/J_{1.5}$ when CS/GR is 20 or below. It is notable that when CS/GR
is 20 or below, $J_3/J_{1.5}$ is even slightly better predicted by theory than J_6/J_3. This is in agreement with Figure 6, which showed
425   a relatively good agreement between the median NPF day $J_3/J_{1.5}$ and L-2007.

If we investigate the observed $J_3/J_{1.5}$ with CS/GR > 20, which diverge from the predictions the most, we can see that the
corresponding values of CS are quite high, while GR are relatively small (Figure 7). In addition, the formation rates,
especially $J_{1.5}$, tend to be high. However, $J_3/J_{1.5}$ with the highest disagreements between the observations and the predictions
430   are mainly characterized by high values of CS. These results indicate that a potential reason for the disagreement between
the observed and the predicted $J_3/J_{1.5}$ is due to CS not corresponding to the actual coagulation scavenging rates during these
events. Another explanations for the disagreement could be considerable underestimation of sub-3 nm GR in high CS
conditions or inhomogeneities in the particle formation. These will be discussed further in Sect. 3.4.3.

435   From Figure 8 we can see that the disagreement between the L-2007, ACDC Case 1 and the observed J_6/J_3 is largest when
CS is low and the disagreement does not seem to vary strongly depending on the value of GR. This supports the possibility
of coagulation between sub-10 nm particles at low CS having a considerable effect on the survivability of particles between
3 and 6 nm. However, current research does not support self-coagulation having such a large contribution to the observed
values of survival probabilities as the required concentrations of sub-10 nm particles are high (Anttila et al., 2010; Yue et al.,
440   2010). In our simulations, the concentrations of sub-3 nm particles need to exceed $3 \cdot 10^6$ cm^{-3} before the values of ACDC
Case 2 survival probabilities are considerably lower than the values of ACDC Case 1 and the L-2007 survival probabilities
due to cluster-cluster collisions. Based on previous studies, the concentrations of cluster and nucleation mode particles in
Beijing during NPF event days are an order of magnitude lower than that (Zhou et al., 2020; Cai et al., 2021b), although the
concentrations contain high uncertainties (Kangasluoma et al., 2020). In addition, if self-coagulation of sub-10 nm particles
445   does lower atmospheric survival probabilities, we would assume it to also be evident at smaller sizes. Despite this, it is still
possible that self-coagulation does influence the observed survival probabilities to some extent and more research is needed

to quantify the effect of population dynamics such as cluster-cluster collisions on survival probabilities of sub-10 nm particles.

3.4.3 Effect of uncertainties and assumptions on survival probabilities

450   J, GR and CS are determined based on measured particle number size distributions. There can be considerable uncertainties in the measured number size distributions, especially at the sub-10 nm size range (Wiedensohler et al., 2012; Kangasluoma et al., 2020). CS in Beijing is dominated by accumulation mode particles and the uncertainty of the measured particle number size distribution in this size range is estimated to be ±10% (Wiedensohler et al., 2012) and we assume that the uncertainty in CS is similar. The uncertainty in the measured particle number size distributions of sub-10 nm particles is

455   significantly higher and has been estimated to be ±50-70% (Kangasluoma et al., 2020). As J in Beijing are mainly contributed by the concentration of new particles and CS (Cai and Jiang, 2017), we assume the uncertainty in J to be in the same range. The uncertainty in GR is also high, and we estimate that it can be up to ±100%. Here, the influence of uncertainty in CS or GR on survival probability is considered. Figures 10 and 11 show the effect of inaccurate CS and GR, correspondingly, on the L-2007 survival probabilities.

460

Based on Figure 10, for $J_3/J_{1.5}$ at CS/GR ≥ 20 CS must be between 50% and 75% lower than assumed to explain the observed values. A large fraction of the observed $J_3/J_{1.5}$ at CS/GR < 20 would also require CS to be less than half of the assumed CS to be explained by the inaccuracy of CS. Most of the observed $J_3/J_{1.5}$ at CS/GR < 20 can be explained if the assumed CS is between 50% lower and 50% higher than the true CS. Assuming that the contribution of self-coagulation is minor, to explain

465   most of the observed J_6/J_3 by inaccuracy of CS, CS must be more than 100% higher. Thus, we argue that the uncertainty of CS due to the uncertainties in the measured particle concentrations cannot solely explain the observed $J_3/J_{1.5}$ or J_6/J_3.

Figure 11 considers the uncertainty of GR instead of the uncertainty of CS. Most of the observed $J_3/J_{1.5}$ at CS/GR < 20 can be explained by GR±50−75%×GR. However, to explain most of the observed $J_3/J_{1.5}$ at CS/GR ≥ 20, and a large fraction at

470   CS/GR < 20, GR would have to be higher by at least 100% and in some cases up to 300%. Thus, while most of the observed $J_3/J_{1.5}$ at CS/GR < 20 can be explained by the uncertainty of GR if GR±100%×GR, a much higher uncertainty is needed to explain most of the observed $J_3/J_{1.5}$ at CS/GR ≥ 20. To explain most of the J_6/J_3 GR would have to be overestimated by 25-75%. Thus, it is possible that the disagreement between the ACDC Case 1, the L-2007 and the observed J_6/J_3 is due to the estimated uncertainty of GR. However, due to the higher uncertainty required to explain the observed $J_3/J_{1.5}$, and the opposite

475   direction of the required inaccuracies, it appears less likely that the uncertainty of GR could also explain, at least fully, the disagreements between the theoretical and the observed $J_3/J_{1.5}$.

CoagS could be overestimated or underestimated if some assumptions made when determining it are inaccurate. We have neglected the enhancement of coagulation due to van der Waals forces, which can result in underestimating CoagS. The van

480   der Waals enhancement of CoagS can be expected to be between 1.0 and 2.0 (Kerminen, 1994). While it cannot alone explain the majority of the observed J_6/J_3 (Figure 10), it could be a part of the reason the observed J_6/J_3 are lower than the ACDC Case 1 and L-2007 J_6/J_3. In addition, all the collisions between new particles and the background particles are assumed to result in coagulation. However, it is possible that only a fraction of all the collisions lead to coagulation due to e.g., chemical properties of the particles. This is analogous to effectiveness of CS in removing condensable vapors such as

485   sulfuric acid (Tuovinen et al., 2021, 2020), which has been shown to be higher for ammonium-nitrate rich background particles (Du et al., 2022). If the effectiveness of CoagS for particles between 1.5 nm and 3 nm varies between 0.25 and 1.0, almost all the observed $J_3/J_{1.5}$ that are larger than predicted based on the simulations or L-2007 can be explained. However, for ineffective CoagS to explain the observed $J_3/J_{1.5}$, the effectiveness of CoagS would have to be strongly size-dependent as the observed values of J_6/J_3 and J_{10}/J_6 do not support CoagS being lower than assumed between 3 nm and 10 nm.

490

In the atmosphere, conditions are constantly changing. We have assumed that GR is constant throughout the event, which can result in inaccuracies in both CS/GR and the survival probabilities themselves. The effects of this assumption on our results are less than straightforward to evaluate. However, for example in Figure 7 the highest disagreements between the predicted and the observed $J_3/J_{1.5}$ are characterized by high CS and thus while the time-dependency of GR might contribute

495   to the disagreements between predictions and observations in some way, it cannot explain the large disagreements for $J_3/J_{1.5}$ at CS/GR ≥ 20. The particle number size distribution of background particles is also constantly changing and while we have accounted for the time-dependency of CS we have not considered the time-dependency of the parameter m but have assumed a constant m of −1.6. We expect the uncertainty from this assumption to be relatively small (see Figure 4) and the effect on our main results to be minor.

500

While NPF events may take place regionally, the air masses where NPF occurs are not completely homogeneous, especially in urban areas with a variety of local emission sources. Because of this the values of CS, GR and J can have spatial variations. For example, GR could on a local scale be higher or lower than what we determine based on the measured particle number size distributions. This can result in locally higher survival rates of sub-10 nm particles, which could affect

505   the observed survival probabilities due to the increased total concentrations of new particles. Increased GR on a local scale could be due to e.g., larger concentrations of precursor vapors due to proximity to emission sources. Wang et al. (2020) and Marten et al. (2022) showed that new particles can grow very rapidly despite high CS and have survival probabilities close to unity in the presence of gas-phase nitric acid and ammonia under controlled laboratory conditions, which could be relevant for inhomogeneous urban environments with local emission sources such as traffic. Thus, while brief but rapid growth of

510   new particles on a small local scale might have no effect on the observed GR at the measurement location it could result in significantly higher values of observed survival probabilities causing apparent discrepancy between the observations and theory.

Another factor relevant to consider in urban environments to consider is the effect of primary particle emissions from traffic
515   on the measured particle number size distributions. Traffic emissions have been shown to significantly contribute to number
concentrations of particles as small as below 3 nm in diameter (Rönkkö et al., 2017). However, Deng et al. (2022) showed
that the influence of traffic emissions on the concentration of sub-3 nm particles at the observation site is negligible
compared to the influence of NPF. Thus, the effect of primary particle and cluster emissions from traffic on $J_3/J_{1.5}$ is likely
minor.

520

We note that it should be considered when interpreting our results that we are only able to observe NPF events when both the
survival probabilities and the formation rates themselves are sufficiently high. Thus, it is likely that our results are biased
towards higher survival probability values, which could make the discrepancy between the observed and the predicted $J_3/J_{1.5}$
appear more significant. If we were also able to accurately describe the growth and formation rates of sub-10 nm particles
525   outside these events, we would have a more complete picture of survival probabilities and their dependency on coagulation
scavenging and particle growth rates in urban Beijing.

Table 2: Root-mean-square logarithmic error and mean absolute logarithmic error between the
observed survival probabilities from 1.5 nm to 3 nm ($J_3/J_{1.5}$), 3 nm to 6 nm (J_6/J_3), and 6 nm to 10 nm
(J_{10s}/J_6) in Beijing, China and theoretical predictions based on formulation by Lehtinen et al. (2007).

	Root-mean-square logarithmic error (CS/GR ≤ 20, CS/GR > 20)	Mean absolute logarithmic error (CS/GR ≤ 20, CS/GR > 20)
$J_3/J_{1.5}$	2.12 (1.25, 3.77)	1.57 (0.96, 3.62)
J_6/J_3	1.32	1.01
J_{10}/J_6	1.28	0.90

4 Conclusions

530   We compared cluster or aerosol particle survival probabilities from 1.5 to 3 nm ($J_3/J_{1.5}$), 3 to 6nm (J_6/J_3), and 6 to 10 nm
(J_{10}/J_6) between predictions based on analytical formulae, cluster population simulations using Atmospheric Cluster
Dynamics Code (ACDC) and observations in Beijing, China, and discussed possible reasons for the corresponding
differences. The survival probabilities based on theory and the cluster population simulations agree relatively well for all of

the three size ranges if no cluster-cluster collisions occur in the simulations or if their contribution to growth and losses of

535 clusters are negligible. However, if CS is low, the inclusion of cluster-cluster collisions in the cluster population simulations results in significantly lower survival probabilities for all the investigated size ranges, and in a weaker dependency of the survival probability on CS due to the increased loss rate of clusters and particles.

A majority of the observed values of $J_3/J_{1.5}$ are higher than those obtained from the cluster population simulations or based

540 on analytical formulae, and the largest discrepancies were observed at high values of CS. At low CS/GR a majority of the observed values of $J_3/J_{1.5}$ can be explained if uncertainties in CS/GR reach approximately ± 75%, a reasonable estimate for an error in atmospheric CS/GR. However, at higher CS/GR the value of CS needs to be lower by more than 50% or the value of GR needs to be higher by more than 100% to explain the observed values of $J_3/J_{1.5}$. Unlike for $J_3/J_{1.5}$, a majority of the observed J_6/J_3 are lower than theoretical J_6/J_3 and the discrepancy is even higher than for $J_3/J_{1.5}$ when CS is low. The

545 disagreement between theoretical and the observed J_6/J_3 can be explained if CS is underestimated by more than 100% or if GR is overestimated by approximately 25-75%. However, the observed J_6/J_3 and J_6/J_3 from the cluster population simulations with cluster-cluster collisions are closer, mostly within a factor of two from each other. The median values of the observed J_{10}/J_6 are relatively close to the theoretical values and to J_{10}/J_6 from the cluster population simulations, both with or without cluster-cluster collisions. However, the variance of these values is high, which we attribute both to measurement

550 uncertainties and to the influence of emissions of sub-10 nm particles to the observed formation rates. Thus, only the survival probability from 1.5 nm to 3 nm appears to be on average higher than predicted under high CS while the survival probabilities between larger sizes did not show a similar trend.

Based on our results it appears unlikely that the effect of cluster-cluster collisions on survival probability explains the

555 observed discrepancies between theory and observations. However, more research is needed to quantify the role of complex dynamic interactions between sub-10 nm particles on survival probability. A reasonable overestimation within the limits of estimated uncertainties in GR can potentially explain the observed values of J_6/J_3 if the influence of cluster-cluster collisions is assumed to be negligible. While a large fraction of the observed values of $J_3/J_{1.5}$ can be explained by the uncertainties of measured CS and GR, it seems probable that at high CS conditions other factors also contribute to the observed survival

560 probabilities. Possible explanations for the observed values of $J_3/J_{1.5}$ under high background particle concentrations include overestimation of CS due to ineffective coagulation scavenging of sub-3 nm particles, or strongly enhanced growth of sub-3 nm particles on a local scale, which is not visible in the observed GR at the measurement location. More research is still required to determine the mechanisms behind enhanced survival probability of below 3 nm particles in polluted conditions.

565 *Data availability*

Theoretical and simulation datasets, and the observed survival probabilities and the corresponding CS and GR will be published at Zenodo.

Author contributions

JK conceptualized the original idea. ST performed the analysis with help from JK, RC, VMK and MK. CY, MK and JJ
570 collected the data. ST prepared and edited the manuscript with contributions from all co-authors.

Competing interests

Author VMK is a member of the editorial board for Atmospheric Chemistry and Physics.

Acknowledgments

575 We acknowledge the following projects: ACCC Flagship funded by the Academy of Finland grant number 337549,
Academy professorship funded by the Academy of Finland (grant no. 302958), Academy of Finland projects no. 1325656,
311932, 316114, 332547,325647, and 332547; "Quantifying carbon sink, CarbonSink+ and their interaction with air quality"
INAR project funded by Jane and Aatos Erkko Foundation, European Research Council (ERC) project ATM-GTP Contract
No. 742206, Technical and scientific staff in Beijing, AHL/BUCT laboratory are acknowledged.

580

585
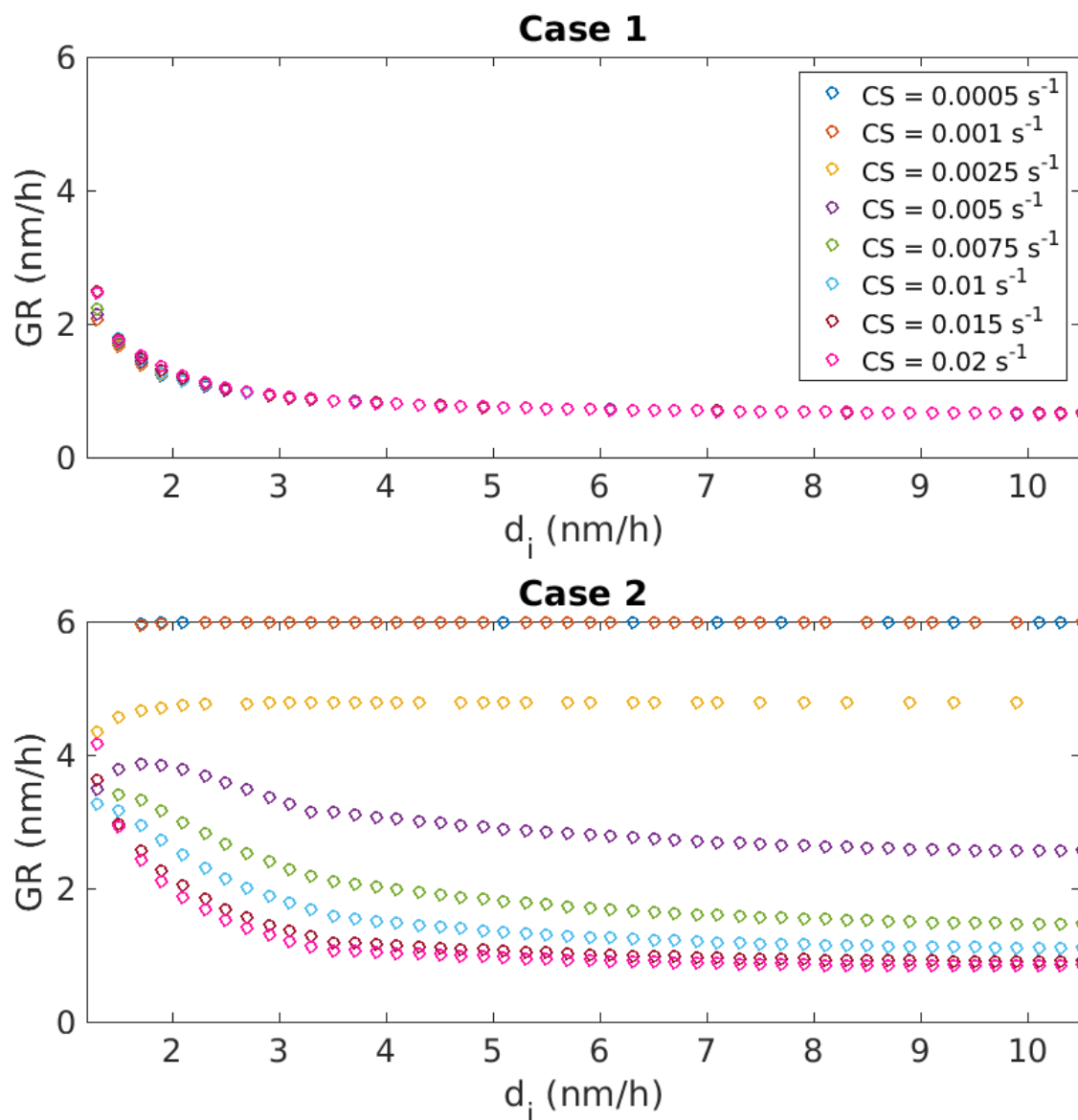
Figure 1: Appearance time method based growth rates (GR) for ACDC simulations with constant monomer concentration $C_{mon} = 10^7$ cm^{-3} as a function of the cluster diameter d_i. GR have been determined based on polynomial regression. Case 1 includes no cluster-cluster collisions while in Case 2 cluster-cluster collision were allowed to occur. Different model runs had different input background condensation sinks (CS) and these have been marked with the different colors.
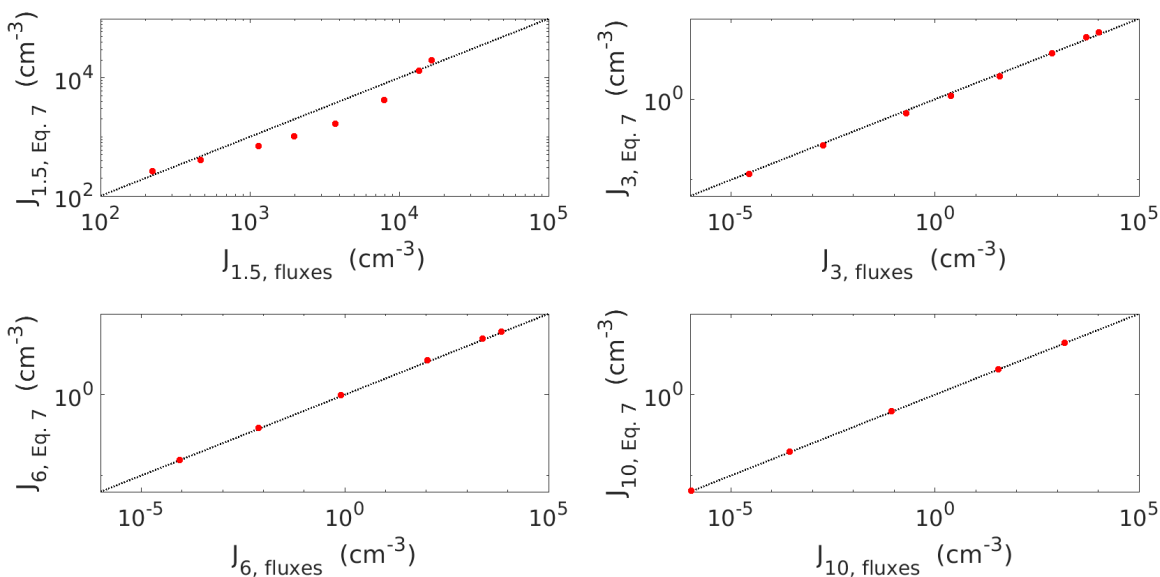
Figure 2: The formation rates (J) from ACDC simulations based on fluxes and Eq. 8 (marked in red) for a case with no cluster-cluster collisions. 1:1 line has been included and is marked with the black dotted line. J are determined at the steady-state and thus in Eq. 8 the change of the cluster number concentration with time is zero.

590
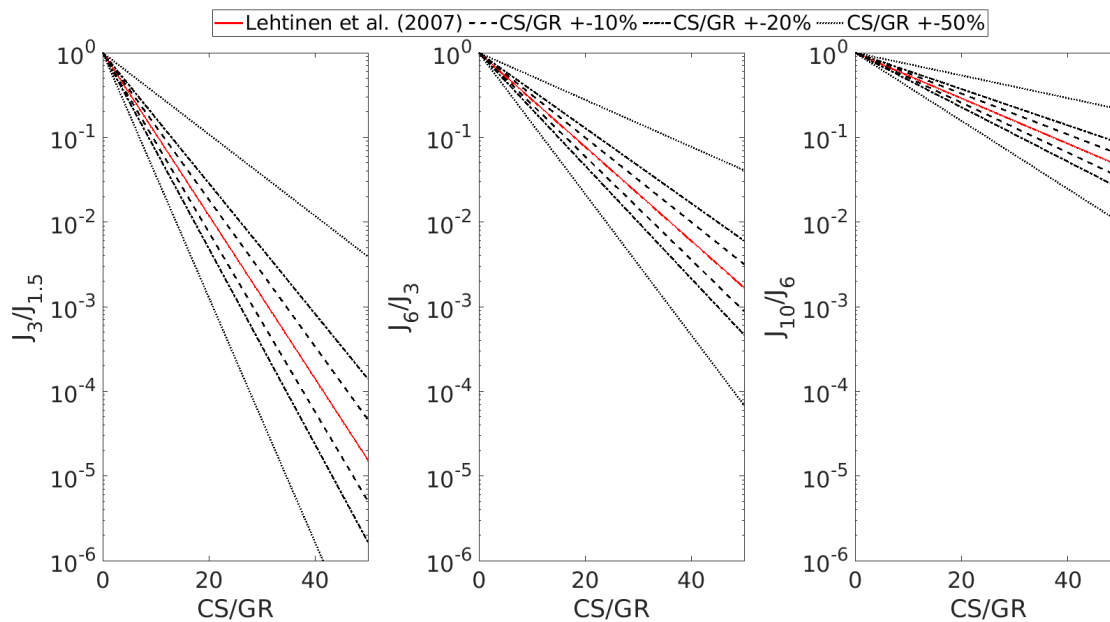
Figure 3: Predictions for the survival probabilities from 1.5 to 3 nm ($J_3/J_{1.5}$), from 3 to 6 nm (J_6/J_3), and 6 to 10 nm (J_{10}/J_6) according to the formulation by Lehtinen et al. (2007). Lines corresponding to the survival probabilities with CS/GR being 10%, 20% and 50% lower, or higher, than assumed are included.
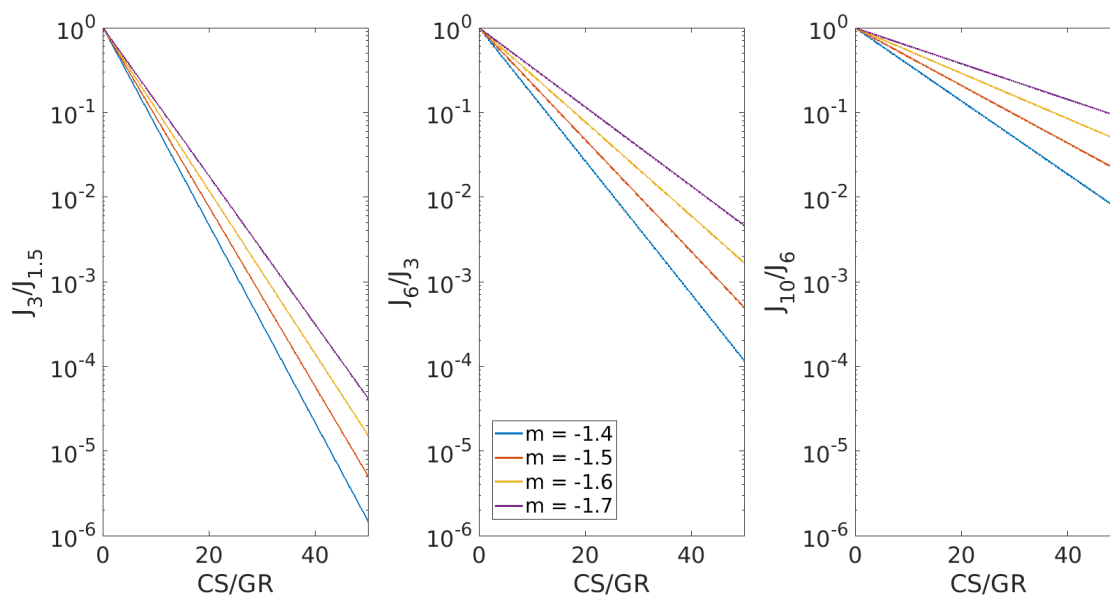
Figure 4: Predictions for the survival probabilities from 1.5 to 3 nm ($J_3/J_{1.5}$), from 3 to 6 nm (J_6/J_3), and 6 to 10 nm (J_{10}/J_6) according to the formulation by Lehtinen et al. (2007). Horizontal axis is the ratio of condensation sink and growth rate (CS/GR). Four different values for the parameter m have been used.
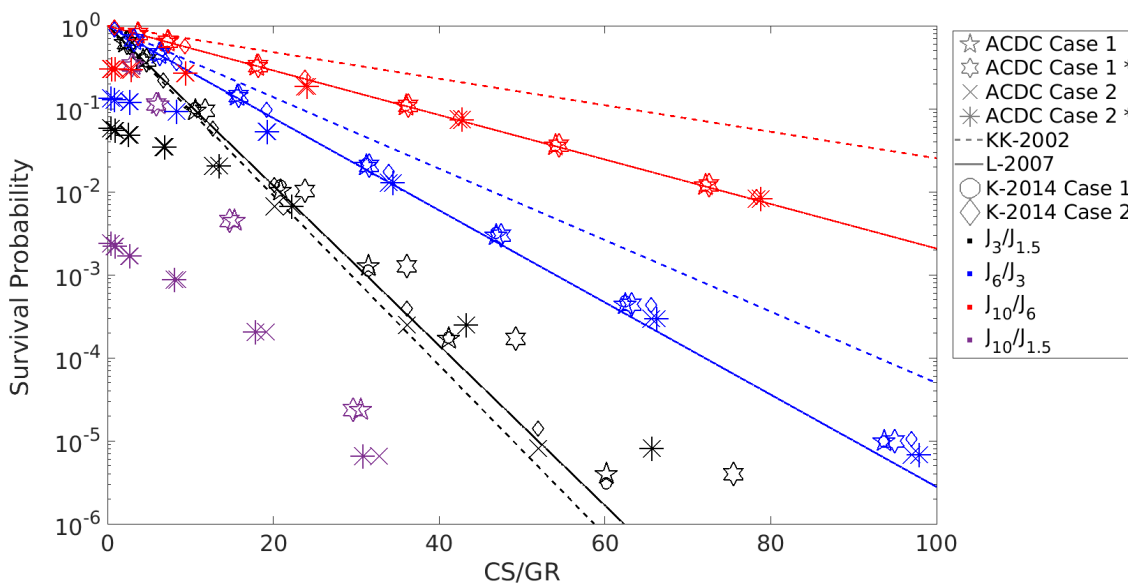
Figure 5: Survival probabilities from 1.5 to 3 nm ($J_3/J_{1.5}$), from 3 to 6 nm (J_6/J_3), from 6 to 10 nm (J_{10}/J_6), and from 1.5 to 10 nm ($J_{10}/J_{1.5}$). Horizontal axis is expressed in terms of background condensation sink of sulfuric acid (CS) and the mean growth rate (GR) in the size range. Survival probabilities based on Atmospheric Cluster Dynamics Code (ACDC) simulation results and theoretical predictions are included. The ACDC survival probabilities are divided to two different cases: in Case 1 no collisions between clusters occur and in Case 2 collisions between clusters are also allowed to occur. In both Case 1 and 2, monomer concentration is $C_{mon} = 1 \cdot 10^7$ cm^{-3}. GR for the values marked with * has been determined based on linear regression while for the other values GR is based on multi-degree polynomial regression. The theoretical predictions are based on Kerminen and Kulmala (2002) (KK-2002) and Lehtinen et al. (2007) (L-2007) formulations, which assume constant GR, and Korhonen et al. (2014) (K-20014) formulation, assuming a power-law size dependency of the GR (see Eq. 1-2).

600
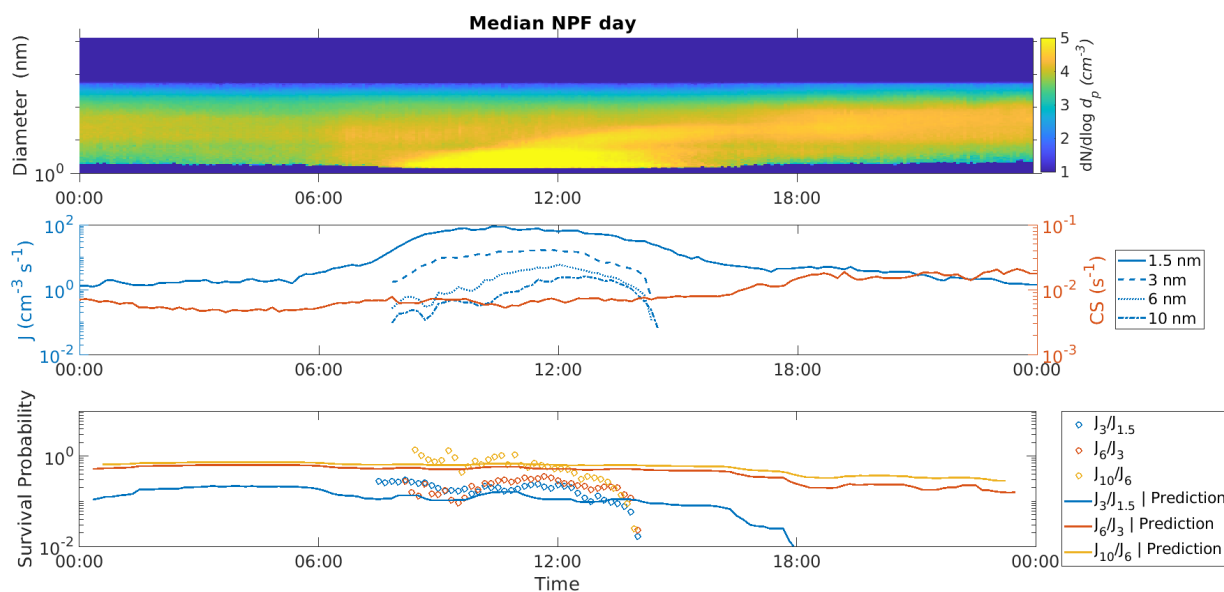
Figure 6: The median particle number size distribution and the median survival probabilities from 1.5 to 3 nm ($J_3/J_{1.5}$), 3 to 6 nm (J_6/J_3) and 6 to 10 nm (J_{10}/J_6) during a NPF event day in Beijing, China. Theoretical predictions for survival probability based on Lehtinen et al. (2007) formulation (see Eq. 2) determined based on the median condensation sink (CS) and the median growth rate (GR) are also shown. The median GR is 2.48 nm/h between 1.5 nm and 3 nm, 4.81 nm/h between 3 nm and 6 nm, and 3.37 nm/h between 6 nm and 10 nm.

605
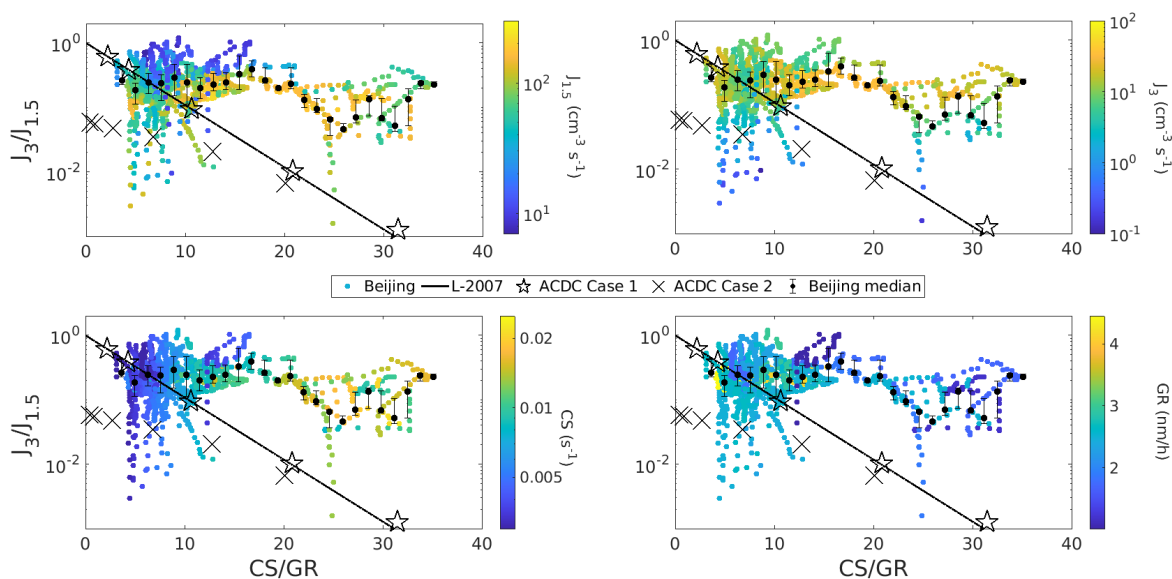
Figure 7: Survival probability from 1.5 nm to 3 nm ($J_3/J_{1.5}$) as a function of the ratio of the condensation sink and the growth rate (CS/GR). Survival probabilities from Beijing, China, the ACDC model simulations and the predictions based on theoretical formulation by Lehtinen et al. (2007) (L-2007) are included. ACDC Case 1 refers to simulations with no collisions between the clusters while in Case 2 simulations cluster-cluster collisions also occurred. The median values for the observed $J_3/J_{1.5}$ have been determined based on a bin division of horizontal values and the quartiles are shown as the error bars. The upper left figure is shaded with the $J_{1.5}$ while the upper right, the bottom left and the bottom right are shaded with the J_3, the CS and the GR correspondingly.

610

615
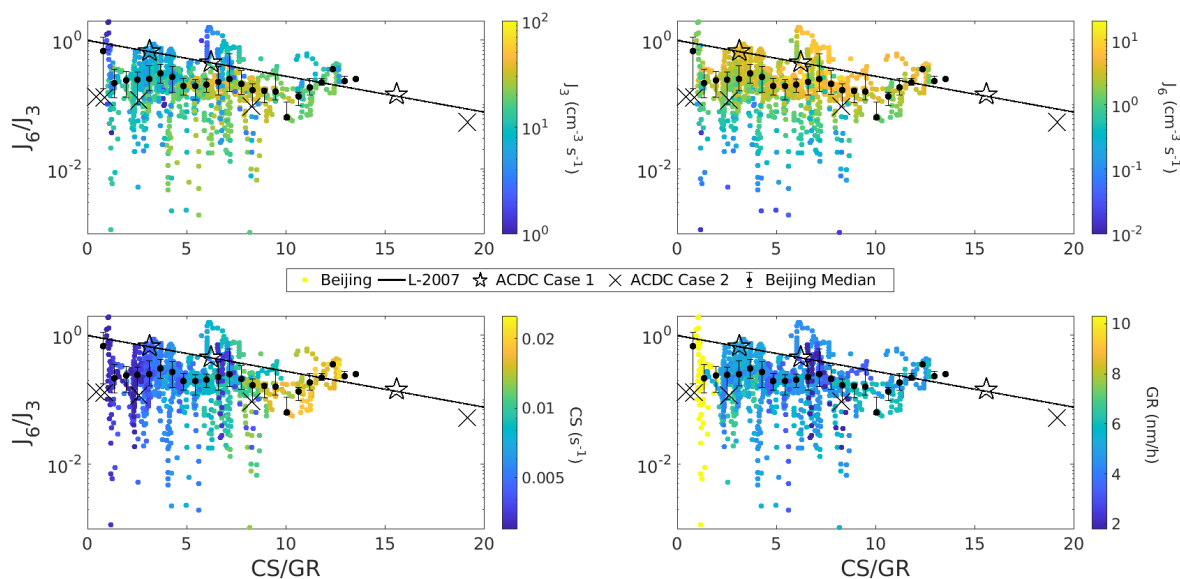
Figure 8: Survival probability from 3 nm to 6 nm (J_6/J_3) as a function of the ratio of condensation sink and growth rate (CS/GR). Survival probabilities from Beijing, China, ACDC model simulations and the predictions based on theoretical formulation by Lehtinen et al. (2007) (L-2007) are included. ACDC Case 1 refers to simulations with no collisions between the clusters while in Case 2 simulations cluster-cluster collisions also occurred. Median values for observed J_6/J_3 have been determined based on a bin division of horizontal values and the quartiles are shown as the error bars. The upper left figure is shaded with the J_3 while the upper right, the bottom left and the bottom right are shaded with the J_6, the CS and the GR correspondingly.

620

625
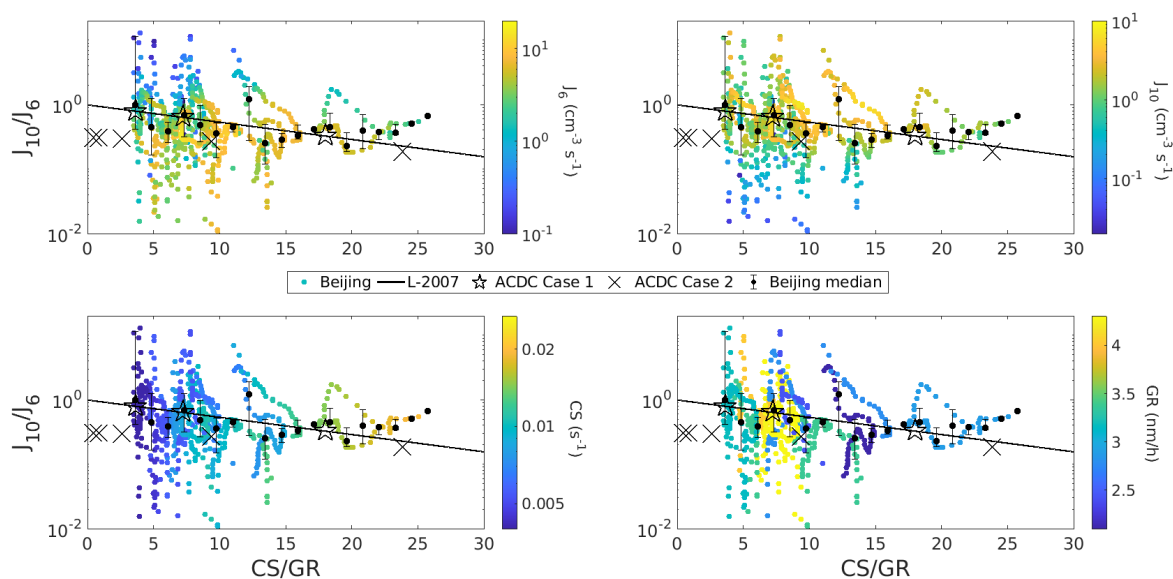
Figure 9: Survival probability from 6 nm to 10 nm (J_{10}/J_6) as a function of the ratio of condensation sink and growth rate (CS/GR). Survival probabilities from Beijing, China, ACDC model simulations and the predictions based on theoretical formulation by Lehtinen et al. (2007) (L-2007) are included. ACDC Case 1 refers to simulations with no collisions between clusters while in Case 2 simulations cluster-cluster collisions also occurred. Median values for observed J_{10}/J_6 have been determined based on bin division of horizontal values and the quartiles are shown as the error bars. The upper left figure is shaded with the J_6 while uthe pper right, bottom left and bottom right are shaded with the J_{10}, the CS and the GR correspondingly.
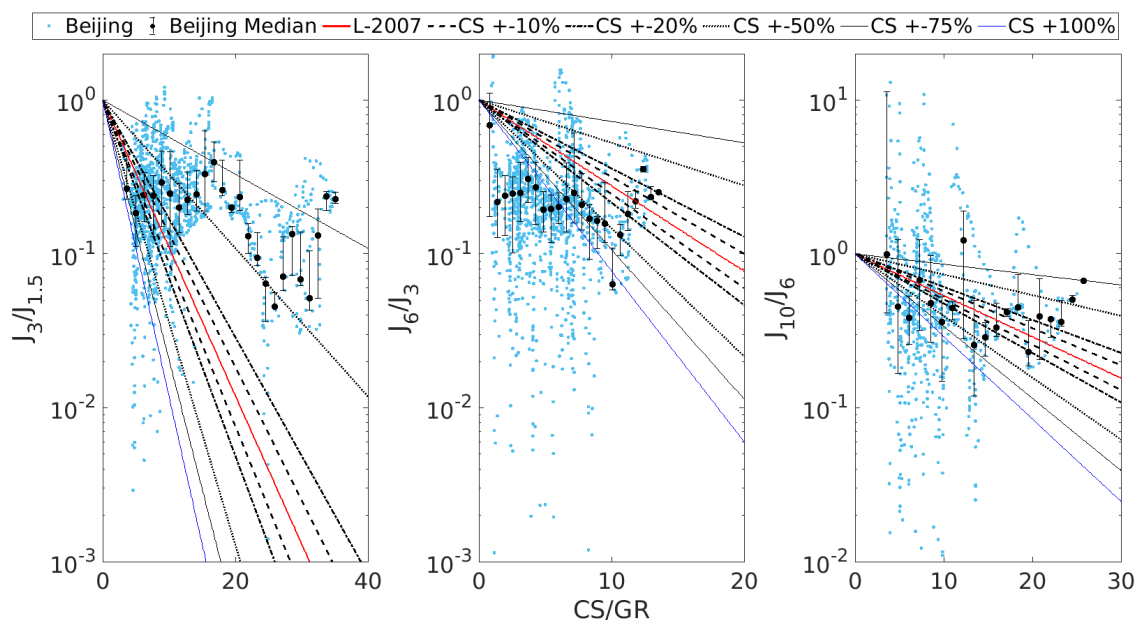
Figure 10: Survival probabilities from 1.5 nm to 3 nm ($J_3/J_{1.5}$), 3 nm to 6 nm (J_6/J_3) and 6 nm to 10 nm (J_{10}/J_6) as a function of the ratio of condensation sink and growth rate (CS/GR). Survival probabilities based on Lehtinen et al. (2007) (L-2007) equation with varying error of CS are presented. The observed survival probabilities from Beijing, China, are shown with their median values marked in black.
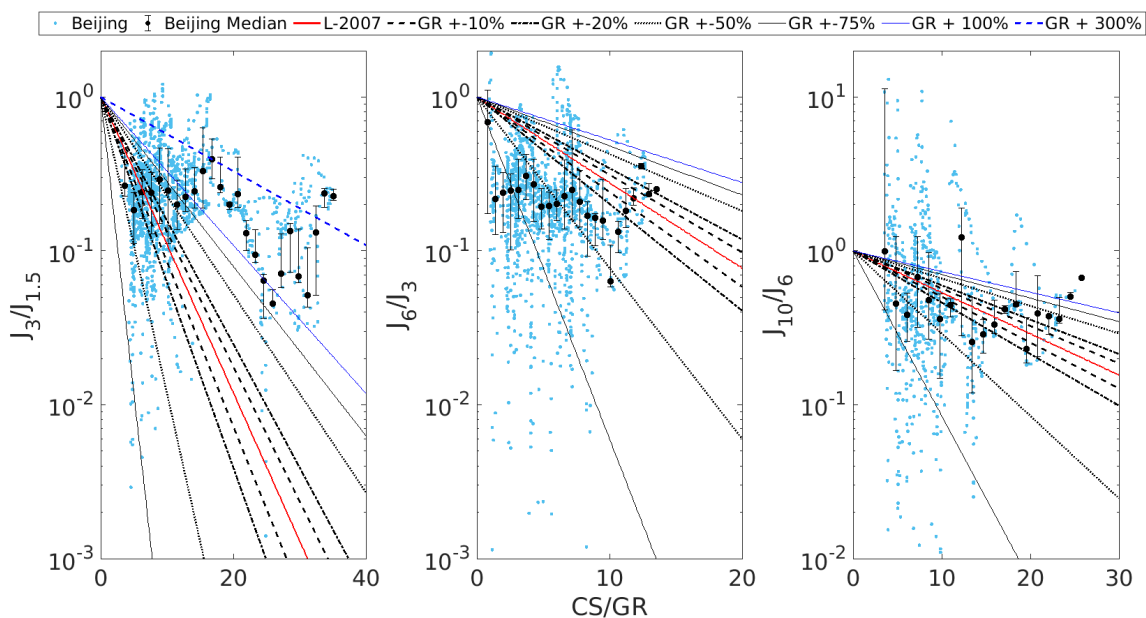
Figure 11: Survival probabilities from 1.5 nm to 3 nm ($J_3/J_{1.5}$), 3 nm to 6 nm (J_6/J_3) and 6 nm to 10 nm (J_{10}/J_6) as a function of the ratio of condensation sink and growth rate (CS/GR). Survival probabilities based on Lehtinen et al. (2007) equation with varying error of GR are presented. The observed survival probabilities from Beijing, China, are shown with their median values marked in black.

635

640

References

Anttila, T., Kerminen, V.-M., Lehtinen, K.E.J., 2010. Parameterizing the formation rate of new particles: The effect of nuclei self-coagulation. Journal of Aerosol Science 41, 621–636. https://doi.org/10.1016/j.jaerosci.2010.04.008

Bellouin, N., Quaas, J., Gryspeerdt, E., Kinne, S., Stier, P., Watson-Parris, D., Boucher, O., Carslaw, K.S., Christensen, M., Daniau, A. -L., Dufresne, J. -L., Feingold, G., Fiedler, S., Forster, P., Gettelman, A., Haywood, J.M., Lohmann, U., Malavelle, F., Mauritsen, T., McCoy, D.T., Myhre, G., Mülmenstädt, J., Neubauer, D., Possner, A., Rugenstein, M., Sato, Y., Schulz, M., Schwartz, S.E., Sourdeval, O., Storelvmo, T., Toll, V., Winker, D., Stevens, B., 2020. Bounding Global Aerosol Radiative Forcing of Climate Change. Rev. Geophys. 58.

Cai, R., Chen, D.-R., Hao, J., Jiang, J., 2017a. A miniature cylindrical differential mobility analyzer for sub-3 nm particle sizing. Journal of Aerosol Science 106, 111–119. https://doi.org/10.1016/j.jaerosci.2017.01.004

Cai, R., Jiang, J., 2017. A new balance formula to estimate new particle formation rate: reevaluating the effect of coagulation scavenging. Atmos. Chem. Phys. 17, 12659–12675. https://doi.org/10.5194/acp-17-12659-2017

Cai, R., Li, C., He, X.-C., Deng, C., Lu, Y., Yin, R., Yan, C., Wang, L., Jiang, J., Kulmala, M., Kangasluoma, J., 2021a. Impacts of coagulation on the appearance time method for new particle growth rate evaluation and their corrections. Atmos. Chem. Phys. 21, 2287–2304. https://doi.org/10.5194/acp-21-2287-2021

Cai, R., Yan, C., Yang, D., Yin, R., Lu, Y., Deng, C., Fu, Y., Ruan, J., Li, X., Kontkanen, J., Zhang, Q., Kangasluoma, J., Ma, Y., Hao, J., Worsnop, D.R., Bianchi, F., Paasonen, P., Kerminen, V.-M., Liu, Y., Wang, L., Zheng, J., Kulmala, M., Jiang, J., 2021b. Sulfuric acid–amine nucleation in urban Beijing. Atmos. Chem. Phys. 21, 2457–2468. https://doi.org/10.5194/acp-21-2457-2021

Cai, R., Yang, D., Fu, Y., Wang, X., Li, X., Ma, Y., Hao, J., Zheng, J., Jiang, J., 2017b. Aerosol surface area concentration: a governing factor in new particle formation in Beijing. Atmos. Chem. Phys. 17, 12327–12340. https://doi.org/10.5194/acp-17-12327-2017

Chu, B., Kerminen, V.-M., Bianchi, F., Yan, C., Petäjä, T., Kulmala, M., 2019. Atmospheric new particle formation in China. Atmospheric Chemistry and Physics 19, 115–138. https://doi.org/10.5194/acp-19-115-2019

Dal Maso, M., Kulmala, M., Lehtinen, K.E.J., Mäkelä, J.M., Aalto, P., O'Dowd, C.D., 2002. Condensation and coagulation sinks and formation of nucleation mode particles in coastal and boreal forest boundary layers. Journal of Geophysical Research: Atmospheres 107, PAR 2-1-PAR 2-10. https://doi.org/10.1029/2001JD001053

Dal Maso, M., Kulmala, M., Riipinen, I., Wagner, R., Hussein, T., Aalto, P.P., Lehtinen, K.E.J., 2005. Formation and growth of fresh atmospheric aerosols: eight years of aerosol size distribution data from SMEAR II, Hyytiälä, Finland. Boreal Environ. Res. 10, 15.

Deng, C., Fu, Y., Dada, L., Yan, C., Cai, R., Yang, D., Zhou, Y., Yin, R., Lu, Y., Li, X., Qiao, X., Fan, X., Nie, W., Kontkanen, J., Kangasluoma, J., Chu, B., Ding, A., Kerminen, V.-M., Paasonen, P., Worsnop, D.R., Bianchi, F., Liu, Y., Zheng, J., Wang, L., Kulmala, M., Jiang, J., 2020. Seasonal Characteristics of New Particle Formation and Growth in Urban Beijing. Environ. Sci. Technol. 54, 8547–8557. https://doi.org/10.1021/acs.est.0c00808

Deng, C., Li, Y., Yan, C., Wu, J., Cai, R., Wang, D., Liu, Y., Kangasluoma, J., Kerminen, V.-M., Kulmala, M., Jiang, J., 2022. Measurement report: Size distributions of urban aerosols down to 1 nm from long-term measurements. Atmospheric Chemistry and Physics Discussions 1–21. https://doi.org/10.5194/acp-2022-414

Du, W., Cai, J., Zheng, F., Yan, C., Zhou, Y., Guo, Y., Chu, B., Yao, L., Heikkinen, L.M., Fan, X., Wang, Y., Cai, R., Hakala, S., Chan, T., Kontkanen, J., Tuovinen, S., Petäjä, T., Kangasluoma, J., Bianchi, F., Paasonen, P., Sun, Y., Kerminen, V.-M., Liu, Y., Daellenbach, K.R., Dada, L., Kulmala, M., 2022. Influence of Aerosol Chemical Composition on Condensation Sink Efficiency and New Particle Formation in Beijing. Environ. Sci. Technol. Lett. 9, 375–382. https://doi.org/10.1021/acs.estlett.2c00159

Fuchs, N.A., Sutugin, A.G., 1971. Highly dispersed aerosols.(Topics in Current Aerosol Research, Vol. 2,) GM Hidy and JR Brock, eds. Pergamon.

Guo, S., Hu, M., Zamora, M.L., Peng, J., Shang, D., Zheng, J., Du, Z., Wu, Z., Shao, M., Zeng, L., Molina, M.J., Zhang, R., 2014. Elucidating severe urban haze formation in China. PNAS 111, 17373–17378. https://doi.org/10.1073/pnas.1419604111

Jen, C.N., McMurry, P.H., Hanson, D.R., 2014. Stabilization of sulfuric acid dimers by ammonia, methylamine, dimethylamine, and trimethylamine. J. Geophys. Res. Atmos. 119, 7502–7514. https://doi.org/10.1002/2014JD021592

Jiang, J., Chen, M., Kuang, C., Attoui, M., McMurry, P.H., 2011. Electrical Mobility Spectrometer Using a Diethylene Glycol Condensation Particle Counter for Measurement of Aerosol Size Distributions Down to 1 nm. Aerosol. Sci. Tech. 45, 510–521. https://doi.org/10.1080/02786826.2010.547538

Kangasluoma, J., Cai, R., Jiang, J., Deng, C., Stolzenburg, D., Ahonen, L.R., Chan, T., Fu, Y., Kim, C., Laurila, T.M., Zhou, Y., Dada, L., Sulo, J., Flagan, R.C., Kulmala, M., Petäjä, T., Lehtipalo, K., 2020. Overview of measurements and current instrumentation for 1–10 nm aerosol particle number size distributions. Journal of Aerosol Science 148, 105584. https://doi.org/10.1016/j.jaerosci.2020.105584

Kerminen, V.-M., 1994. Simulation of Brownian Coagulation in the Presence of van der Waals Forces and Viscous Interactions. Aerosol Science and Technology 20, 207–214. https://doi.org/10.1080/02786829408959677

Kerminen, V.-M., Chen, X., Vakkari, V., Petäjä, T., Kulmala, M., Bianchi, F., 2018. Atmospheric new particle formation and growth: review of field observations. Environ. Res. Lett. 13, 103003. https://doi.org/10.1088/1748-9326/aadf3c

Kerminen, V.-M., Kulmala, M., 2002. Analytical formulae connecting the "real" and the "apparent" nucleation rate and the nuclei number concentration for atmospheric nucleation events. J. Aerosol Sci. 33, 609–622. https://doi.org/10.1016/S0021-8502(01)00194-X

Kontkanen, J., Deng, C., Fu, Y., Dada, L., Zhou, Y., Cai, J., Daellenbach, K.R., Hakala, S., Kokkonen, T.V., Lin, Z., Liu, Y., Wang, Y., Yan, C., Petäjä, T., Jiang, J., Kulmala, M., Paasonen, P., 2020. Size-resolved particle number emissions in Beijing determined from measured particle size distributions. Atmospheric Chemistry and Physics 20, 11329–11348. https://doi.org/10.5194/acp-20-11329-2020

Kontkanen, J., Olenius, T., Kulmala, M., Riipinen, I., 2018. Exploring the potential of nano-Köhler theory to describe the growth of atmospheric molecular clusters by organic vapors using cluster kinetics simulations. Atmospheric Chemistry and Physics 18, 13733–13754. https://doi.org/10.5194/acp-18-13733-2018

Kontkanen, J., Stolzenburg, D., Olenius, T., Yan, C., Dada, L., Ahonen, L., Simon, M., Lehtipalo, K., Riipinen, I., 2022. What controls the observed size-dependency of the growth rates of sub-10 nm atmospheric particles? Environmental Science: Atmospheres. https://doi.org/10.1039/D1EA00103E

Kulmala, M., Cai, R., Stolzenburg, D., Zhou, Y., Dada, L., Guo, Y., Yan, C., Petäjä, T., Jiang, J., Kerminen, V.-M., 2022. The contribution of new particle formation and subsequent growth to haze formation. Environ. Sci.: Atmos. https://doi.org/10.1039/D1EA00096A

Kulmala, M., Dada, L., Daellenbach, K.R., Yan, C., Stolzenburg, D., Kontkanen, J., Ezhova, E., Hakala, S., Tuovinen, S., Kokkonen, T.V., Kurppa, M., Cai, R., Zhou, Y., Yin, R., Baalbaki, R., Chan, T., Chu, B., Deng, C., Fu, Y., Ge, M., He, H., Heikkinen, L., Junninen, H., Liu, Yiliang, Lu, Y., Nie, W., Rusanen, A., Vakkari, V., Wang, Y., Yang, G., Yao, L., Zheng, J., Kujansuu, J., Kangasluoma, J., Petäjä, T., Paasonen, P., Järvi, L., Worsnop, D., Ding, A., Liu, Yongchun, Wang, L., Jiang, J., Bianchi, F., Kerminen, V.-M., 2021. Is reducing new particle formation a plausible solution to mitigate particulate air pollution in Beijing and other Chinese megacities? Faraday Discuss. 226, 334–347. https://doi.org/10.1039/D0FD00078G

Kulmala, M., Kerminen, V.-M., Petäjä, T., Ding, A.J., Wang, L., 2017. Atmospheric gas-to-particle conversion: why NPF events are observed in megacities? Faraday Discuss. 200, 271–288. https://doi.org/10.1039/C6FD00257A

Kulmala, M., Maso, M.D., Mäkelä, J.M., Pirjola, L., Väkevä, M., Aalto, P., Miikkulainen, P., Hämeri, K., O'dowd, C.D., 2001. On the formation, growth and composition of nucleation mode particles. Tellus B 53, 479–490. https://doi.org/10.1034/j.1600-0889.2001.530411.x

Kulmala, M., Petäjä, T., Mönkkönen, P., Koponen, I.K., Dal Maso, M., Aalto, P.P., Lehtinen, K.E.J., Kerminen, V.-M., 2005. On the growth of nucleation mode particles: source rates of condensable vapor in polluted and clean environments. Atmos. Chem. Phys. 5, 409–416. https://doi.org/10.5194/acp-5-409-2005

Kulmala, M., Petäjä, T., Nieminen, T., Sipilä, M., Manninen, H.E., Lehtipalo, K., Dal Maso, M., Aalto, P.P., Junninen, H., Paasonen, P., Riipinen, I., Lehtinen, K.E.J., Laaksonen, A., Kerminen, V.-M., 2012. Measurement of the nucleation of atmospheric aerosol particles. Nat. Protoc. 7, 1651–1667. https://doi.org/10.1038/nprot.2012.091

Kürten, A., Jokinen, T., Simon, M., Sipilä, M., Sarnela, N., Junninen, H., Adamov, A., Almeida, J., Amorim, A., Bianchi, F., Breitenlechner, M., Dommen, J., Donahue, N.M., Duplissy, J., Ehrhart, S., Flagan, R.C., Franchin, A., Hakala, J., Hansel, A., Heinritzi, M., Hutterli, M., Kangasluoma, J., Kirkby, J., Laaksonen, A., Lehtipalo, K., Leiminger, M., Makhmutov, V., Mathot, S., Onnela, A., Petäjä, T., Praplan, A.P., Riccobono, F., Rissanen, M.P., Rondo, L., Schobesberger, S., Seinfeld, J.H., Steiner, G., Tomé, A., Tröstl, J., Winkler, P.M., Williamson, C., Wimmer, D., Ye, P., Baltensperger, U., Carslaw, K.S., Kulmala, M., Worsnop, D.R., Curtius, J., 2014. Neutral molecular cluster formation of sulfuric acid–dimethylamine observed in real time under atmospheric conditions. PNAS 111, 15019–15024. https://doi.org/10.1073/pnas.1404853111

Lehtinen, K.E.J., Dal Maso, M., Kulmala, M., Kerminen, V.-M., 2007. Estimating nucleation rates from apparent particle formation rates and vice versa: Revised formulation of the Kerminen–Kulmala equation. J. Aerosol Sci. 38, 988–994. https://doi.org/10.1016/j.jaerosci.2007.06.009

Lehtipalo, K., Leppä, J., Kontkanen, J., Kangasluoma, J., Franchin, A., Wimmer, D., Schobesberger, S., Junninen, H., Petäjä, T., Sipilä, M., Mikkilä, J., Vanhanen, J., Worsnop, D.R., Kulmala, M., 2014. Methods for determining particle size distribution and growth rates between 1 and 3 nm using the Particle Size Magnifier. Boreal Env. Res. 19, 215–236.

Lehtipalo, K., Rondo, L., Kontkanen, J., Schobesberger, S., Jokinen, T., Sarnela, N., Kürten, A., Ehrhart, S., Franchin, A., Nieminen, T., Riccobono, F., Sipilä, M., Yli-Juuti, T., Duplissy, J., Adamov, A., Ahlm, L., Almeida, J., Amorim, A., Bianchi, F., Breitenlechner, M., Dommen, J., Downard, A.J., Dunne, E.M., Flagan, R.C., Guida, R., Hakala, J., Hansel, A., Jud, W., Kangasluoma, J., Kerminen, V.-M., Keskinen, H., Kim, J., Kirkby, J., Kupc, A., Kupiainen-Määttä, O., Laaksonen, A., Lawler, M.J., Leiminger, M., Mathot, S., Olenius, T., Ortega, I.K., Onnela, A., Petäjä, T., Praplan, A., Rissanen, M.P., Ruuskanen, T., Santos, F.D., Schallhart, S., Schnitzhofer, R., Simon, M., Smith, J.N., Tröstl, J., Tsagkogeorgas, G., Tomé, A., Vaattovaara, P., Vehkamäki, H., Vrtala, A.E., Wagner, P.E., Williamson, C., Wimmer, D., Winkler, P.M., Virtanen, A., Donahue, N.M., Carslaw, K.S., Baltensperger, U., Riipinen, I., Curtius, J., Worsnop, D.R., Kulmala, M., 2016. The effect of acid–base clustering and ions on the growth of atmospheric nano-particles. Nat. Commun. 7, 11594. https://doi.org/10.1038/ncomms11594

Li, X., Zhao, B., Zhou, W., Shi, H., Yin, R., Cai, R., Yang, D., Dällenbach, K., Deng, C., Fu, Y., Qiao, X., Wang, L., Liu, Y., Yan, C., Kulmala, M., Zheng, J., Hao, J., Wang, S., Jiang, J., 2020. Responses of gaseous sulfuric acid and particulate sulfate to reduced SO2 concentration: A perspective from long-term measurements in Beijing. Science of The Total Environment 721, 137700. https://doi.org/10.1016/j.scitotenv.2020.137700

Liu, J., Jiang, J., Zhang, Q., Deng, J., Hao, J., 2016. A spectrometer for measuring particle size distributions in the range of 3 nm to 10 μm. Front. Environ. Sci. Eng. 10, 63–72. https://doi.org/10.1007/s11783-014-0754-x

Lu, Y., Yan, C., Fu, Y., Chen, Y., Liu, Yiliang, Yang, G., Wang, Y., Bianchi, F., Chu, B., Zhou, Y., Yin, R., Baalbaki, R., Garmash, O., Deng, C., Wang, W., Liu, Yongchun, Petäjä, T., Kerminen, V.-M., Jiang, J., Kulmala, M., Wang, L., 2019. A proxy for atmospheric daytime gaseous sulfuric acid concentration in urban Beijing. Atmospheric Chemistry and Physics 19, 1971–1983. https://doi.org/10.5194/acp-19-1971-2019

Marten, R., Xiao, M., Rörup, B., Wang, M., Kong, W., He, X.-C., Stolzenburg, D., Pfeifer, J., Marie, G., S. Wang, D., Scholz, W., Baccarini, A., Ping Lee, C., Amorim, A., Baalbaki, R., M. Bell, D., Bertozzi, B., Caudillo, L., Chu, B., Dada, L., Duplissy, J., Finkenzeller, H., Gonzalez Carracedo, L., Granzin, M., Hansel, A., Heinritzi, M., Hofbauer, V., Kemppainen, D., Kürten, A., Lampimäki, M., Lehtipalo, K., Makhmutov, V., E. Manninen, H., Mentler, B., Petäjä, T., Philippov, M., Shen, J., Simon, M., Stozhkov, Y., Tomé, A., C. Wagner, A., Wang, Y., K. Weber, S., Wu, Y., Zauner-Wieczorek, M., Curtius, J., Kulmala, M., Möhler, O., Volkamer, R., M. Winkler, P., R. Worsnop, D., Dommen, J., C. Flagan, R., Kirkby, J., M. Donahue, N., Lamkaddam, H., Baltensperger, U., Haddad, I.E., 2022. Survival of newly formed particles in haze conditions. Environmental Science: Atmospheres. https://doi.org/10.1039/D2EA00007E

McGrath, M.J., Olenius, T., Ortega, I.K., Loukonen, V., Paasonen, P., Kurtén, T., Kulmala, M., Vehkamäki, H., 2012. Atmospheric Cluster Dynamics Code: a flexible method for solution of the birth-death equations. Atmospheric Chemistry and Physics 12, 2345–2355. https://doi.org/10.5194/acp-12-2345-2012

Nieminen, T., Lehtinen, K.E.J., Kulmala, M., 2010. Sub-10 nm particle growth by vapor condensation – effects of vapor molecule size and particle thermal speed. Atmos. Chem. Phys. 10, 9773–9779. https://doi.org/10.5194/acp-10-9773-2010

Olenius, T., Riipinen, I., 2017. Molecular-resolution simulations of new particle formation: Evaluation of common assumptions made in describing nucleation in aerosol dynamics models. Aerosol Science and Technology 51, 397–408. https://doi.org/10.1080/02786826.2016.1262530

Olenius, T., Riipinen, I., Lehtipalo, K., Vehkamäki, H., 2014. Growth rates of atmospheric molecular clusters based on appearance times and collision–evaporation fluxes: Growth by monomers. Journal of Aerosol Science 78, 55–70. https://doi.org/10.1016/j.jaerosci.2014.08.008

Pierce, J.R., Adams, P.J., 2007. Efficiency of cloud condensation nuclei formation from ultrafine particles. Atmos. Chem. Phys. 7, 1367–1379. https://doi.org/10.5194/acp-7-1367-2007

Pöschl, U., 2005. Atmospheric Aerosols: Composition, Transformation, Climate and Health Effects. Angewandte Chemie International Edition 44, 7520–7540. https://doi.org/10.1002/anie.200501122

Rönkkö, T., Kuuluvainen, H., Karjalainen, P., Keskinen, J., Hillamo, R., Niemi, J.V., Pirjola, L., Timonen, H.J., Saarikoski, S., Saukko, E., Järvinen, A., Silvennoinen, H., Rostedt, A., Olin, M., Yli-Ojanperä, J., Nousiainen, P., Kousa, A., Dal Maso, M., 2017. Traffic is a major source of atmospheric nanocluster aerosol. Proceedings of the National Academy of Sciences 114, 7549–7554. https://doi.org/10.1073/pnas.1700830114

Rosenfeld, D., Sherwood, S., Wood, R., Donner, L., 2014. Climate Effects of Aerosol-Cloud Interactions. Science 343, 379–380. https://doi.org/10.1126/science.1247490

Shiraiwa, M., Ueda, K., Pozzer, A., Lammel, G., Kampf, C.J., Fushimi, A., Enami, S., Arangio, A.M., Fröhlich-Nowoisky, J., Fujitani, Y., Furuyama, A., Lakey, P.S.J., Lelieveld, J., Lucas, K., Morino, Y., Pöschl, U., Takahama, S., Takami, A., Tong, H., Weber, B., Yoshino, A., Sato, K., 2017. Aerosol Health Effects from Molecular to Global Scales. Environ Sci Technol 51, 13545–13567. https://doi.org/10.1021/acs.est.7b04417

Sihto, S.-L., Kulmala, M., Kerminen, V.-M., Dal Maso, M., Petäjä, T., Riipinen, I., Korhonen, H., Arnold, F., Janson, R., Boy, M., Laaksonen, A., Lehtinen, K.E.J., 2006. Atmospheric sulphuric acid and aerosol formation: implications from atmospheric measurements for nucleation and early growth mechanisms. Atmospheric Chemistry and Physics 6, 4079–4091. https://doi.org/10.5194/acp-6-4079-2006

Spracklen, D.V., Carslaw, K.S., Kulmala, M., Kerminen, V.-M., Sihto, S.-L., Riipinen, I., Merikanto, J., Mann, G.W., Chipperfield, M.P., Wiedensohler, A., Birmili, W., Lihavainen, H., 2008. Contribution of particle formation to global cloud condensation nuclei concentrations. Geophysical Research Letters 35. https://doi.org/10.1029/2007GL033038

Spracklen, D.V., Carslaw, K.S., Merikanto, J., Mann, G.W., Reddington, C.L., Pickering, S., Ogren, J.A., Andrews, E., Baltensperger, U., Weingartner, E., Boy, M., Kulmala, M., Laakso, L., Lihavainen, H., Kivekäs, N., Komppula, M., Mihalopoulos, N., Kouvarakis, G., Jennings, S.G., O'Dowd, C., Birmili, W., Wiedensohler, A., Weller, R., Gras, J., Laj, P., Sellegri, K., Bonn, B., Krejci, R., Laaksonen, A., Hamed, A., Minikin, A., Harrison, R.M., Talbot, R., Sun, J., 2010. Explaining global surface aerosol number concentrations in terms of primary emissions and particle formation. Atmos. Chem. Phys. 10, 4775–4793. https://doi.org/10.5194/acp-10-4775-2010

Stolzenburg, D., Simon, M., Ranjithkumar, A., Kürten, A., Lehtipalo, K., Gordon, H., Ehrhart, S., Finkenzeller, H., Pichelstorfer, L., Nieminen, T., He, X.-C., Brilke, S., Xiao, M., Amorim, A., Baalbaki, R., Baccarini, A., Beck, L., Bräkling, S., Caudillo Murillo, L., Chen, D., Chu, B., Dada, L., Dias, A., Dommen, J., Duplissy, J., El Haddad, I., Fischer, L., Gonzalez Carracedo, L., Heinritzi, M., Kim, C., Koenig, T.K., Kong, W., Lamkaddam, H., Lee, C.P., Leiminger, M., Li, Z., Makhmutov, V., Manninen, H.E., Marie, G., Marten, R., Müller, T., Nie, W., Partoll, E., Petäjä, T., Pfeifer, J., Philippov, M., Rissanen, M.P., Rörup, B., Schobesberger, S., Schuchmann, S., Shen, J., Sipilä, M., Steiner, G., Stozhkov, Y., Tauber, C., Tham, Y.J., Tomé, A., Vazquez-Pufleau, M., Wagner, A.C., Wang, M., Wang, Y., Weber, S.K., Wimmer, D., Wlasits, P.J., Wu, Y., Ye, Q., Zauner-Wieczorek, M., Baltensperger, U.,

Carslaw, K.S., Curtius, J., Donahue, N.M., Flagan, R.C., Hansel, A., Kulmala, M., Lelieveld, J., Volkamer, R., Kirkby, J., Winkler, P.M., 2020. Enhanced growth rate of atmospheric particles from sulfuric acid. Atmos. Chem. Phys. 20, 7359–7372. https://doi.org/10.5194/acp-20-7359-2020

Stolzenburg, M.R., McMurry, P.H., Sakurai, H., Smith, J.N., Mauldin III, R.L., Eisele, F.L., Clement, C.F., 2005. Growth rates of freshly nucleated atmospheric particles in Atlanta. Journal of Geophysical Research: Atmospheres 110. https://doi.org/10.1029/2005JD005935

Tuovinen, S., Kontkanen, J., Cai, R., Kulmala, M., 2021. Condensation sink of atmospheric vapors: the effect of vapor properties and the resulting uncertainties. Environmental Science: Atmospheres 1, 543–557. https://doi.org/10.1039/D1EA00032B

Tuovinen, S., Kontkanen, J., Jiang, J., Kulmala, M., 2020. Investigating the effectiveness of condensation sink based on heterogeneous nucleation theory. Journal of Aerosol Science 149, 105613. https://doi.org/10.1016/j.jaerosci.2020.105613

Wang, M., Kong, W., Marten, R., He, X.-C., Chen, D., Pfeifer, J., Heitto, A., Kontkanen, J., Dada, L., Kürten, A., Yli-Juuti, T., Manninen, H.E., Amanatidis, S., Amorim, A., Baalbaki, R., Baccarini, A., Bell, D.M., Bertozzi, B., Bräkling, S., Brilke, S., Murillo, L.C., Chiu, R., Chu, B., De Menezes, L.-P., Duplissy, J., Finkenzeller, H., Carracedo, L.G., Granzin, M., Guida, R., Hansel, A., Hofbauer, V., Krechmer, J., Lehtipalo, K., Lamkaddam, H., Lampimäki, M., Lee, C.P., Makhmutov, V., Marie, G., Mathot, S., Mauldin, R.L., Mentler, B., Müller, T., Onnela, A., Partoll, E., Petäjä, T., Philippov, M., Pospisilova, V., Ranjithkumar, A., Rissanen, M., Rörup, B., Scholz, W., Shen, J., Simon, M., Sipilä, M., Steiner, G., Stolzenburg, D., Tham, Y.J., Tomé, A., Wagner, A.C., Wang, D.S., Wang, Y., Weber, S.K., Winkler, P.M., Wlasits, P.J., Wu, Y., Xiao, M., Ye, Q., Zauner-Wieczorek, M., Zhou, X., Volkamer, R., Riipinen, I., Dommen, J., Curtius, J., Baltensperger, U., Kulmala, M., Worsnop, D.R., Kirkby, J., Seinfeld, J.H., El-Haddad, I., Flagan, R.C., Donahue, N.M., 2020. Rapid growth of new atmospheric particles by nitric acid and ammonia condensation. Nature 581, 184–189. https://doi.org/10.1038/s41586-020-2270-4

Wang, Z.B., Hu, M., Pei, X.Y., Zhang, R.Y., Paasonen, P., Zheng, J., Yue, D.L., Wu, Z.J., Boy, M., Wiedensohler, A., 2015. Connection of organics to atmospheric new particle formation and growth at an urban site of Beijing. Atmos. Environ. 103, 7–17. https://doi.org/10.1016/j.atmosenv.2014.11.069

Wiedensohler, A., Birmili, W., Nowak, A., Sonntag, A., Weinhold, K., Merkel, M., Wehner, B., Tuch, T., Pfeifer, S., Fiebig, M., Fjäraa, A.M., Asmi, E., Sellegri, K., Depuy, R., Venzac, H., Villani, P., Laj, P., Aalto, P., Ogren, J.A., Swietlicki, E., Williams, P., Roldin, P., Quincey, P., Hüglin, C., Fierz-Schmidhauser, R., Gysel, M., Weingartner, E., Riccobono, F., Santos, S., Grüning, C., Faloon, K., Beddows, D., Harrison, R., Monahan, C., Jennings, S.G., O'Dowd, C.D., Marinoni, A., Horn, H.-G., Keck, L., Jiang, J., Scheckman, J., McMurry, P.H., Deng, Z., Zhao, C.S., Moerman, M., Henzing, B., de Leeuw, G., Löschau, G., Bastian, S., 2012. Mobility particle size spectrometers: harmonization of technical standards and data structure to facilitate high quality long-term observations of atmospheric particle number size distributions. Atmospheric Measurement Techniques 5, 657–685. https://doi.org/10.5194/amt-5-657-2012

Wu, Z., Hu, M., Lin, P., Liu, S., Wehner, B., Wiedensohler, A., 2008. Particle number size distribution in the urban atmosphere of Beijing, China. Atmospheric Environment 42, 7967–7980. https://doi.org/10.1016/j.atmosenv.2008.06.022

Xiao, M., Hoyle, C.R., Dada, L., Stolzenburg, D., Kürten, A., Wang, M., Lamkaddam, H., Garmash, O., Mentler, B., Molteni, U., Baccarini, A., Simon, M., He, X.-C., Lehtipalo, K., Ahonen, L.R., Baalbaki, R., Bauer, P.S., Beck, L., Bell, D., Bianchi, F., Brilke, S., Chen, D., Chiu, R., Dias, A., Duplissy, J., Finkenzeller, H., Gordon, H., Hofbauer, V., Kim, C., Koenig, T.K., Lampilahti, J., Lee, C.P., Li, Z., Mai, H., Makhmutov, V., Manninen, H.E., Marten, R., Mathot, S., Mauldin, R.L., Nie, W., Onnela, A., Partoll, E., Petäjä, T., Pfeifer, J., Pospisilova, V., Quéléver, L.L.J., Rissanen, M., Schobesberger, S., Schuchmann, S., Stozhkov, Y., Tauber, C., Tham, Y.J., Tomé, A., Vazquez-Pufleau, M., Wagner, A.C., Wagner, R., Wang, Y., Weitz, L., Wimmer, D., Wu, Y., Yan, C., Ye, P., Ye, Q., Zha, Q., Zhou, X., Amorim, A., Carslaw, K., Curtius, J., Hansel, A., Volkamer, R., Winkler, P.M., Flagan, R.C., Kulmala, M., Worsnop, D.R., Kirkby, J., Donahue, N.M., Baltensperger, U., El Haddad, I., Dommen, J., 2021. The

driving factors of new particle formation and growth in the polluted boundary layer. Atmospheric Chemistry and Physics 21, 14275–14291. https://doi.org/10.5194/acp-21-14275-2021

Yao, L., Garmash, O., Bianchi, F., Zheng, J., Yan, C., Kontkanen, J., Junninen, H., Mazon, S.B., Ehn, M., Paasonen, P., Sipilä, M., Wang, M., Wang, X., Xiao, S., Chen, H., Lu, Y., Zhang, B., Wang, D., Fu, Q., Geng, F., Li, L., Wang, H., Qiao, L., Yang, X., Chen, J., Kerminen, V.-M., Petäjä, T., Worsnop, D.R., Kulmala, M., Wang, L., 2018. Atmospheric new particle formation from sulfuric acid and amines in a Chinese megacity. Science 361, 278–281. https://doi.org/10.1126/science.aao4839

Yue, D.L., Hu, M., Zhang, R.Y., Wang, Z.B., Zheng, J., Wu, Z.J., Wiedensohler, A., He, L.Y., Huang, X.F., Zhu, T., 2010. The roles of sulfuric acid in new particle formation and growth in the mega-city of Beijing. Atmos. Chem. Phys. 10, 4953–4960. https://doi.org/10.5194/acp-10-4953-2010

Yue, D.L., Hu, M., Zhang, R.Y., Wu, Z.J., Su, H., Wang, Z.B., Peng, J.F., He, L.Y., Huang, X.F., Gong, Y.G., Wiedensohler, A., 2011. Potential contribution of new particle formation to cloud condensation nuclei in Beijing. Atmospheric Environment 45, 6070–6077. https://doi.org/10.1016/j.atmosenv.2011.07.037

Zhou, Y., Dada, L., Liu, Yiliang, Fu, Y., Kangasluoma, J., Chan, T., Yan, C., Chu, B., Daellenbach, K.R., Bianchi, F., Kokkonen, T.V., Liu, Yongchun, Kujansuu, J., Kerminen, V.-M., Petäjä, T., Wang, L., Jiang, J., Kulmala, M., 2020. Variation of size-segregated particle number concentrations in wintertime Beijing. Atmos. Chem. Phys. 20, 1201–1216. https://doi.org/10.5194/acp-20-1201-2020